Project acronym:	**GeoSmart**		
Project title:	Technologies for geothermal to enhance competitiveness in smart and flexible operation		
Activity:	LC-SC3-RES-12-2018		
Call:	H2020-LC-SC3-2018-RES-SingleStage		
Funding Scheme:	IA	**Grant Agreement No:**	818576
WP	**4 – Development of scaling reduction system**		

D4.3 – Report on preliminary design of HX including materials compatibility investigation

Due date:	31/07/2021 (M16)	
Actual Submission Date:	30/07/2021 (M16)	
Lead Beneficiary:	CEA	
Main authors/contributors:	N Caney, S Rougé, B Holmes, A Sabard, C Lee	
Dissemination Level[1]:	Public	
Nature:	Report	
Status of this version:		**Draft under Development**
		For Review by Coordinator
	X	**Submitted**
Version:	V1	
Abstract	This deliverable reports the development of the pre-design of a heat exchanger for the site of Kizildere 2 in Turkey. A plate and gasket heat exchanger was selected as the most optimised design to minimise fouling, and material compatibility with the geothermal brine was investigated for a selection of 5 potential candidates.	

REVISION HISTORY

Version	Date	Main Authors/Contributors	Description of changes
V1	29/07/21	N Caney, S Rougé, B Holmes, A Sabard, C Lee	

[1] Dissemination level security:

PU – Public (e.g. on website, for publication etc.) / **PP** – Restricted to other programme participants (incl. Commission services) /

RE – Restricted to a group specified by the consortium (incl. Commission services) / **CO** – confidential, only for members of the consortium (incl. Commission services)

This project has received funding from the *European Union's Horizon 2020 research and innovation programme* under grant agreement No 818576

This project has received funding from the European Union's Horizon 2020 program Grant Agreement No 818576. This publication reflects the views only of the author(s), and the Commission cannot be held responsible for any use which may be made of the information contained therein.

Copyright © 2019-2023, GeoSmart Consortium

This document and its contents remain the property of the beneficiaries of the GeoSmart Consortium and may not be distributed or reproduced without the express written approval of the GeoSmart Coordinator, TWI Ltd. (www.twi-global.com)

THIS DOCUMENT IS PROVIDED BY THE COPYRIGHT HOLDERS AND CONTRIBUTORS "AS IS" AND ANY EXPRESS OR IMPLIED WARRANTIES, INCLUDING, BUT NOT LIMITED TO, THE IMPLIED WARRANTIES OF MERCHANTABILITY AND FITNESS FOR A PARTICULAR PURPOSE ARE DISCLAIMED. IN NO EVENT SHALL THE COPYRIGHT OWNER OR CONTRIBUTORS BE LIABLE FOR ANY DIRECT, INDIRECT, INCIDENTAL, SPECIAL, EXEMPLARY, OR CONSEQUENTIAL DAMAGES (INCLUDING, BUT NOT LIMITED TO, PROCUREMENT OF SUBSTITUTE GOODS OR SERVICES; LOSS OF USE, DATA, OR PROFITS; OR BUSINESS INTERRUPTION) HOWEVER CAUSED AND ON ANY THEORY OF LIABILITY, WHETHER IN CONTRACT, STRICT LIABILITY, OR TORT (INCLUDING NEGLIGENCE OR OTHERWISE) ARISING IN ANY WAY OUT OF THE USE OF THIS DOCUMENT, EVEN IF ADVISED OF THE POSSIBILITY OF SUCH DAMAGE.

Acronyms

Ar	Argon
ASTM	American Society for Testing and Materials
CRA	Corrosion resistant alloy
DPI	Dye penetrant inspection
HX	Heat exchanger
KPI	Key performance indicator
M6	Metric 6mm thread
P&ID	Piping and instrumentation diagram
SCC	Stress corrosion cracking
UNS	Unified numbering system

Summary

This deliverable reports the pre-design of the heat exchanger that will be installed on the site of Kizildere II in Turkey. A manufacturer with the help of the CEA will design the HX.

- It concerns a plate and gasket heat exchanger.
- The schematic P&ID is detailed as well as the operating conditions that have been considered to design the HX for WP4.
- The heat-exchanger is optimised to minimise scaling and fouling
- The present document includes the instrumentation for detection of fouling

The report also includes the materials compatibility investigation conducted by TWI.

- Crevice corrosion, pitting corrosion and stress-corrosion cracking tests were performed
- 304L, 254SMO (UNS S31254), 316L, UNS S32760 and Ti Grade 1 and 2 were tested
- Conditions were based on Kizildere II brine after the low-pressure separator
- Long-term autoclave testing and short-term electrochemical testing was performed
- Detailed post-test evaluation was conducted
- Anti-fouling coatings were not investigated because it is unfeasible to coat the selected HX geometry

The work detailed in this deliverable contributes towards meeting the KPI detailed in D1.8 [1].

Objectives Met

The deliverable contributed towards the work package objective:

- To create the initial design of a heat exchanger with capability to cool the brine to a temperature around 50°C.
- To provide instrumentation to detect and measure fouling in HX.
- To perform specific tests on materials to ensure that the brine is compatible with the selected materials

CONTENTS

ACRONYMS 4

SUMMARY 4

OBJECTIVES MET 4

1. INTRODUCTION 7

2. AVAILABLE GEOMETRIES OF HX 7

1.1. SHELL AND TUBE HEAT EXCHANGERS 7

1.2. PLATE HEAT EXCHANGERS 8

1.3. SELECTION OF THE TECHNOLOGY 8

3. HEAT EXCHANGER SPECIFICATIONS 9

4. MATERIAL COMPATIBILITY 11

4.1 LITERATURE REVIEW 11

4.2 MATERIALS AND METHODS 13

4.2.1 Material 13

4.2.2 Sample preparation 14

4.2.2.1 Crevice corrosion 14

4.2.2.2 Stress-corrosion cracking specimens 14

4.2.3 Electrochemical testing 15

4.2.4 Environment and experimental design 15

4.2.4.1 Brine recipe 15

4.2.4.2 Tests 1 and 2 – long-term exposure in simulated geothermal brine 16

4.2.4.3 Tests 3 and 4 – potentiodynamic scans 18

4.2.5 Post-test characterisation 21

4.2.5.1 Visual examination 21

4.2.5.2 Mass loss 21

4.2.5.3 Optical profilometry 21

4.2.5.4 Scanning electron microscopy (SEM) 21

4.3 CHEMICAL COMPATIBILITY RESULTS 21

4.3.1 Crevice corrosion 21

4.3.2 U-bends 22

4.3.3 Potentiodynamic scans 23

4.4 CONCLUSIONS OF CORROSION TESTING 27

5. FOULING DETECTION 28

6. PRE SIZING AND CHARACTERISTICS OF THE HEAT EXCHANGER 29

7. DATA OVERVIEW FINAL DESIGN 34

8. CONCLUSIONS 34

9. REFERENCES 35

APPENDIX A – Results Sheets for crevice corrosion specimens

APPENDIX B – Results Sheets for u-bend specimens

APPENDIX C – Results Sheets for Potentiodynamic Scan

1. INTRODUCTION

The aim of WP4 is to develop and optimise a scaling reduction system for the Zorlu Kizildere II demonstrator.
The objective is to recover more heat from the process in order to supply a district heating system or greenhouses. The risk in decreasing the temperature, which is currently reinjected at 104°C, is to create deposits in the reinjection well.
The objective of WP4 is therefore twofold: to show that heat can be recovered, if possible up to 50°C, while avoiding deposits. The silica could even be recovered.

Task 4.3 concerns the design of the HX and the investigations on materials to limit scaling.

CEA will design a full heat exchanger compatible with the conditions at Zorlu demonstration site. The design will ensure a highly efficient exchange to cool the brine rapidly so that the silica deposit only occurs in the retention tank. CEA will define, procure and implement specific sensors on the heat exchanger on site with associated electronics to recover the measurement of fouling.

TWI has performed corrosion testing on five corrosion resistant alloy (CRA) candidate materials for the HX at temperatures relevant to the minimum and maximum operating and design temperatures of the HX. Long-term static crevice corrosion and stress corrosion cracking testing were performed to simulate the likely failure modes and evaluate scaling. Short-term electrochemical testing was performed to assess the likelihood of pitting corrosion in the simulated geothermal brine.

2. AVAILABLE GEOMETRIES OF HX

Among the different types of heat exchangers, **shell and tube** heat exchangers are preferred for space heating, power production, and chemical processing applications. The main advantages of this heat exchanger type over other types can be listed as follows:

- There is substantial flexibility regarding their materials to accommodate corrosion and other concerns;
- They can be used in systems with higher operating temperatures and pressures;
- Tube leaks are easily located and plugged since pressure test is comparatively easy.

However, this kind of heat exchanger requires more space, and cleaning and maintenance are difficult since a tube requires sufficient amount of clearance at one end to remove the tube nest.

Although not a standard practice, use of **plate heat exchangers** instead, may be a tempting option due to their compact size, their mass production (lower cost), ease of dismantling/reassembly, ease of cleaning, and their high overall heat transfer coefficient, typical values of which are 10-20 kW/m².

The most relevant heat exchangers for large-scale geothermal power plants are **shell-and-tube heat exchangers**. However **plate-type heat exchangers** are most cost-effective (lower heat transfer surface) and have many advantages for the specific application. Thus, next section compares the two technologies in terms of thermal performances, costs and scaling.

1.1. Shell and tube heat exchangers

The main fluid circulates inside the tubes to homogeneously flow. The speed increasing can reduce the deposition. It is also necessary to have a good distribution on the shell side (installation of baffles) in order to limit hot or cold areas. Thus, it is necessary to take care of the distribution of the fluid at the level of the tubular plate to avoid any risk of by-pass.

This configuration also has the advantage of being relatively easy to clean. However, the U-tube configuration is excluded, as it does not allow mechanical or hydraulic cleaning of the tubes.

For the design of shell and tube heat exchanger, it is recommended to:

- Use a reduced space between the baffles and the shell to prevent a significant part of the flow from short-circuiting the bundle
- Use a baffle opening of about 20% of the shell diameter
- Have a uniform speed in the bundle
- Preferably use a square-pitch bundle to facilitate manual cleaning
- Avoid dead and recirculation zones, especially at the exchanger connections

1.2. Plate heat exchangers

Plate heat exchangers are used up to pressures of 20 bars and temperatures of 200 °C for mainly single-phase liquid applications. There are compact heat exchangers with high thermal efficiencies, lower costs and less dead and recirculation zones.

Plate heat exchangers behave better towards scaling than other types of exchangers:

- Higher turbulence induced between the plates keeps the fine solid particles in suspension ;
- The surface quality of the plates is better than that of the tubes;
- There are few dead areas where the fluid is almost stagnant;
- The cleaning of the exchanger is easy by chemical process or by plate disassembly when manual cleaning is required.

1.3. Selection of the technology

A comparison between available options is summarised in **Error! Reference source not found.**.

Table 1: Comparison of two technologies available of heat exchangers

Feedback from experience:

Type of heat exchanger	Field of application Pressure Temperature	Fouling behaviour	Easy cleaning
Shell and tube	Almost limitless	Average, better on tube side	Good on tube side, average on shell side
Plate and gaskets	20 bars 200°C	Good	Easy

Scaling :

Type of heat exchanger	Advantages	Drawbacks
Shell and tube	No dead zones in the tubes, uniform speed, used in geothermic (why?), easy removal of the tubes	Cost, obstruction of the tubes, kinetics knowledge, fouling sensors set up during assemblage process
Plate and gaskets	Compact, lower cost, less dead and recirculation zones, fouling sensors set up after assemblage process, easy cleaning	Deposit at the exit, leakage of the device

Following the presentation of these elements, the meeting at Kizildere (14-15 January 2020) acted that a **plate and gasket heat exchanger** was the **most relevant** technology.

3. HEAT EXCHANGER SPECIFICATIONS

The meeting at Kizildere (14-15 January 2020) decided that a plate heat-exchanger was the best technology and that a residence time of a few seconds would allow to have no scaling inside the heat-exchanger (UoI kinetics model). It was therefore decided to decrease the brine temperature **down to 50°C instead of 70°C**, while maintaining the brine flowrate.

The thermal power of the HX is 3 MW.

Some data are still required (mainly maximal pressure drop on brine and water sides and final pressure level on brine side) to optimise the design. The CEA has set these values in order to make a pre design calculation.

To help understanding the heat exchangers design, a simplified scheme of the facilities that will be set up at Kizildere II is illustrated below:

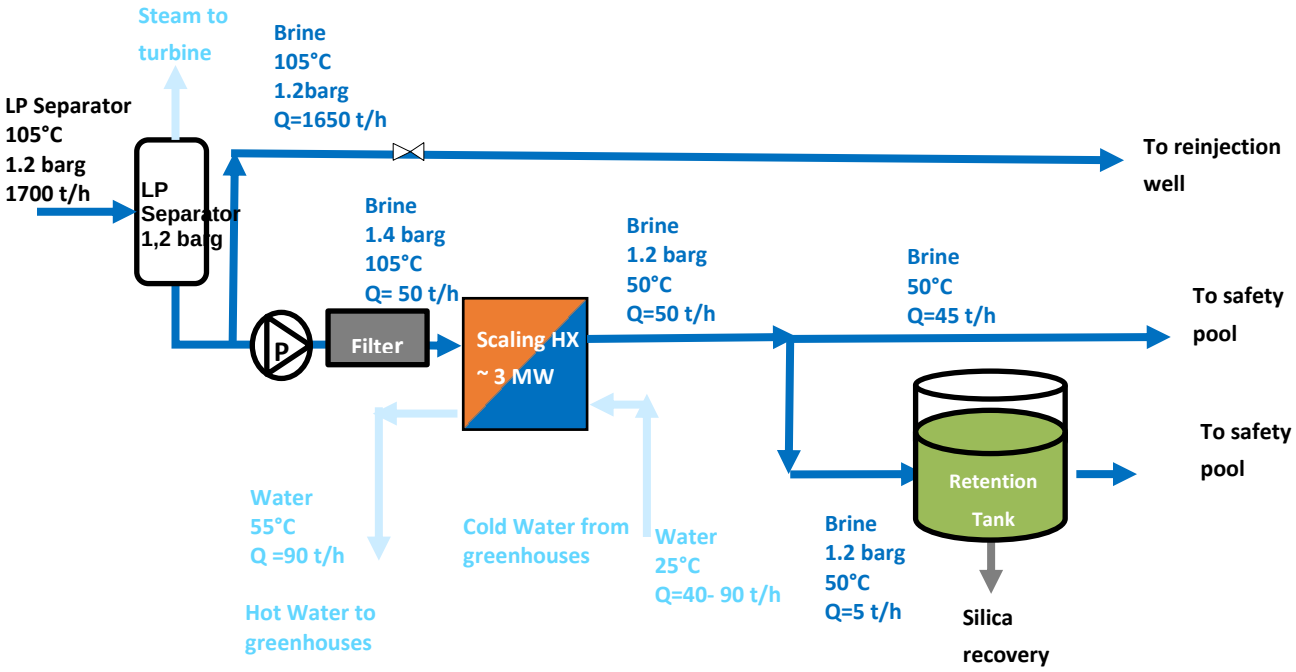

Figure 1 : Simplified PI&D of the test rig at Kizildere II

In this diagram, the following components are missing stop and control valves and the associated pressure drops.

The specifications of each circuit are detailed in the following table:

Table 2 KIZILDERE II specifications for HX

	Hot side Brine	Cold side Water
Flow rate kg/h	50 000	90 000
Inlet temperature °C	105	25
Nominal inlet pressure	> 1.2 barg 1.4 barg	1 barg
Outlet temperature °C	50 *A sizing point at 70-80 will be requested*	50-55
Maximum pressure drop (mbar)	200	200
Design pressure	4 barg 7 barg possible	4 barg 7 barg possible
Power MW	3	

or

Circuit	Fluid	Pressure	Temp. inlet [°C]	Temp. outlet [°C]	Flow rate [t/h]	Max allowable pressure
Brine circuit (dark blue)	Brine	1.4 barg	105	50-70	50	9 barg
Water circuit (light blue)	Water	1 barg	20-25	50-55	40-90	9 barg

CEA is also looking for specifications outside the nominal point, i.e. to be able to get out hotter on the primary side if there is too much fouling. We could aim for 70°C for example, by changing only the flow rate on the secondary side. Indeed, the idea of a lower secondary flow rate to keep power constant has been investigated and proposed to ZORLU (cf. Figure 2):

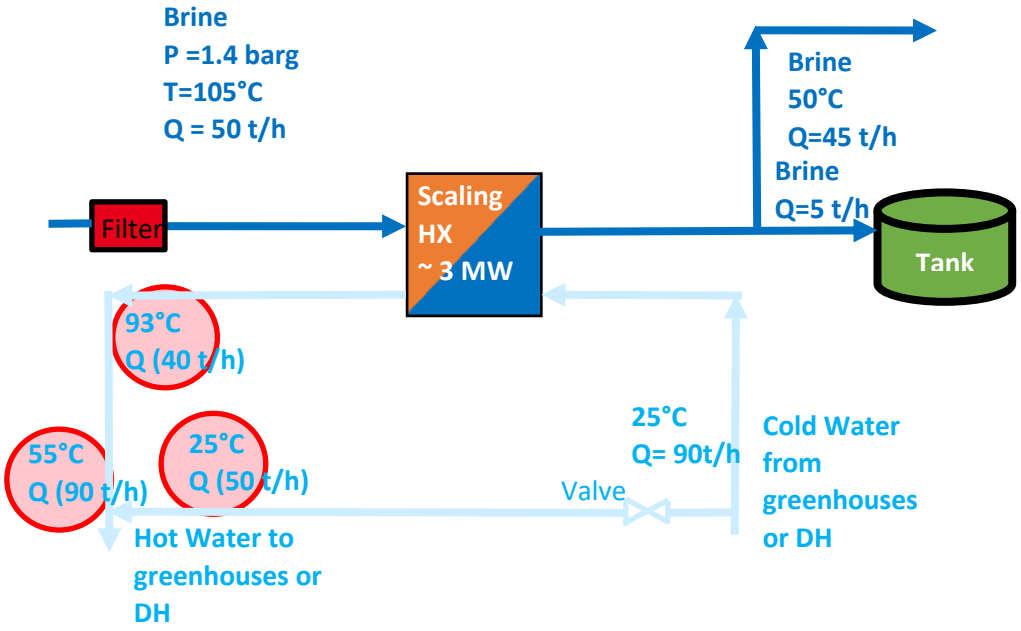

Figure 2 : Simplified PI&D of the test rig at Kizildere II: option of a lower secondary flow rate

In this configuration, if the HX becomes reasonably fouled on the primary side, by gradually closing the valve, the secondary flow in the HX increases: the power is maintained. The flow rate and temperature of the secondary after mixing with the bypass are unchanged (90 t/h, 55°C). Flexibility is in the transition from 40 t/h to 50 t/h.

4. MATERIAL COMPATIBILITY

4.1 Literature review

Published literature was briefly reviewed for typical materials for heat exchangers and their corrosion performance in geothermal environments. It is important to note that corrosion tests may be performed in the laboratory or in the field. Laboratory testing enables control of individual parameters, and thus understanding of their effects, but it can be difficult to include the effects of all parameters such as trace minerals and gases, flow and suspended solids. The benefit of field testing is that all real parameters, including associated variations in conditions can be evaluated [2]

Review of published corrosion test results and experience can be valuable, but it is important to look for data generated under similar environmental conditions (eg brine composition, pH, temperature). There are many geothermal fields in the world, and due to the number of environmental variables, there is a vast range of different corrosivities and therefore, material selection guidelines can also vary widely. The conditions at Zorlu are low chloride, pH>9, and significant amounts of silica are present. Chloride is corrosive to many metals and alloys, and silica can act as an inhibitor [3]. In addition, Mg, Ca and other scaling anions are present (Table 3). Published corrosion data for similar conditions were sought, with the Kizildere II conditions fitting broadly into 'Geothermal Resource Corrosion Class V' [3], and subgroup Va [4], see Table 4. Moreover, Table 4 shows the published corrosion data for such fields. Further, regarding corrosion performance in similar environment, Ellis [3] stated that 'Type 316 stainless steel is resistant to uniform corrosion, pitting and crevice corrosion, and stress corrosion cracking in many applications'. Uniform and pitting corrosion of carbon steel were observed in nonaerated fluids, with aeration reported to increase corrosion rates by a factor of 10 from typically <1mpy for pH>9.

Table 3 Geothermal Resource Corrosion Class V Subgroup Va [4]

Parameter	Value
Resource type	Liquid dominated
Total key species (TKS)	<5000ppm
Chloride	3-72%
pH (unflashed fluid)	6.7-7.6
Plant inlet temperature	120-205°F (~49-96°C)
Total alkalinity	207-1329 ppm $CaCO_3$

Table 4 Published corrosion data

Reference	Field	Country	Comments
[5]	Onikobe, Mori, Kakkonda,	Japan	All low chloride, >pH9 (ALL WELL DATA)
[3]	Hveragerdi, Hengill, Svartsengi	Iceland	Svartsengi used titanium and stainless steel plate heat exchanger. Few corrosion problems were reported.
[3]	Klamath Falls	Oregon, USA	Lower Si than Kizildere; 2mils max pit depth after 6 months, 304. Eg p329
[3,4]	Madison Aquifer	South Dakota, USA	Lower SiO_2 than Kizildere (21-42ppm used for corrosion tests). Titanium showed no detectable corrosion at Diamond Ring Bar-N Ranch. 304 and 316 stainless steels exhibited crevice corrosion. 304 exhibited pitting corrosion.
[4]	Pagosa Springs	Colorado, USA	
[4]	Marlin	Texas, USA	

Typical failure mechanisms of heat exchangers include localised corrosion and environmental cracking. Crevice corrosion is a risk where plates are mechanically joined, and the residual stresses from manufacturing and clamping within a plate and gasket heat exchanger could potentially give rise to a risk of stress corrosion cracking at the elevated temperature observed within a heat exchanger.

Long-term testing is useful as it allows testing conditions to be more realistic than those in accelerated short-term tests. However, due to the limited time available to perform extensive long-term testing, both long-term immersion testing and short-term electrochemical testing were performed. Potentiodynamic scans provide a short-term method of assessing the corrosion behavior of alloys, by providing information on passive current density and pitting potential. All tests were static, and did not consider flowing conditions. Static conditions tend to be worse for corrosion of stainless steels.

Although fouling and silica deposition remain a challenge in geothermal powerplants, options are available to prevent this phenomenon from happening, from module design modifications to brine alteration (pH, temperature). Conditions to limit fouling were ultimately chosen by partners based on flow and retention time [6]. While coatings application and surface engineering were considered to mitigate the scaling, options available such as thermal spray or epoxy paints require respectively line of sight or application by hand. Neither of these options are applicable in the pre-selected heat exchanger geometries as the brine is either flowing inside corrugations of the plate and gasket module or inside the tube of a tube and shell system.

Hydrogen effects on materials were considered, but not tests were performed because temperatures were above those where hydrogen embrittlement is typically encountered and below those where high temperature hydrogen attack would be encountered. It was considered that there would be little or no hydrogen in the stream within the heat exchanger, unless considerable corrosion were to occur.

4.2 Materials and Methods

4.2.1 Material

A selection of five substrates were selected to be tested as part of D4.3 to investigate their corrosion performance in a simulated geothermal brine consistent with the composition of Kizildere II fluid. The materials that were tested are detailed in Table 5. Not all materials were tested in all types of test. Duplicate specimens were tested in most cases in order to give reassurance of the test result.

Table 5 Materials tested

Material	***UNS***	***Reason for selection***
Superduplex stainless steel	UNS S32760	Classical material for heat exchanger
304/304L	UNS S30403	The general-purpose grade, widely used where good formability and corrosion resistance are required.
316L	UNS S31603	As 304L but with molybdenum added to increase resistance to localised corrosion in marine and chemical environments
254 SMO	UNS S31254	Superaustenitic stainless steel with excellent corrosion and stress corrosion cracking resistance to chloride environments
Ti grade 2	UNS R50400	Typical applications for Grade 2 titanium are oil and gas components, reaction and pressure vessels, as well as heat exchangers

4.2.2 Sample preparation

4.2.2.1 Crevice corrosion

In order to investigate the potential crevice corrosion behavior of the selected material in the simulated brine environment, crevice formers were clamped onto 50x20x5 mm coupons. Each crevice former had 20 crevices, equaling a total of 40 crevices per sample, as the formers were placed on both sides of the specimens. The coupons were drilled according to the drawing shown in Figure 3(a), to accommodate the presence of the crevice former (bottom hole) and the sample stand (top hole). A 7.5 mm clearance hole was drilled to accommodate the M6 Ti grade 2 bolts holding the crevice formers. Samples were immersed in tap water prior to assembly, and were then installed using a special wrench to a torque of 0.28Nm, in accordance with ASTM G48 Method D. Electrical isolation between bolts and specimens was ensured, and the samples were kept in tap water until insertion in the autoclave.

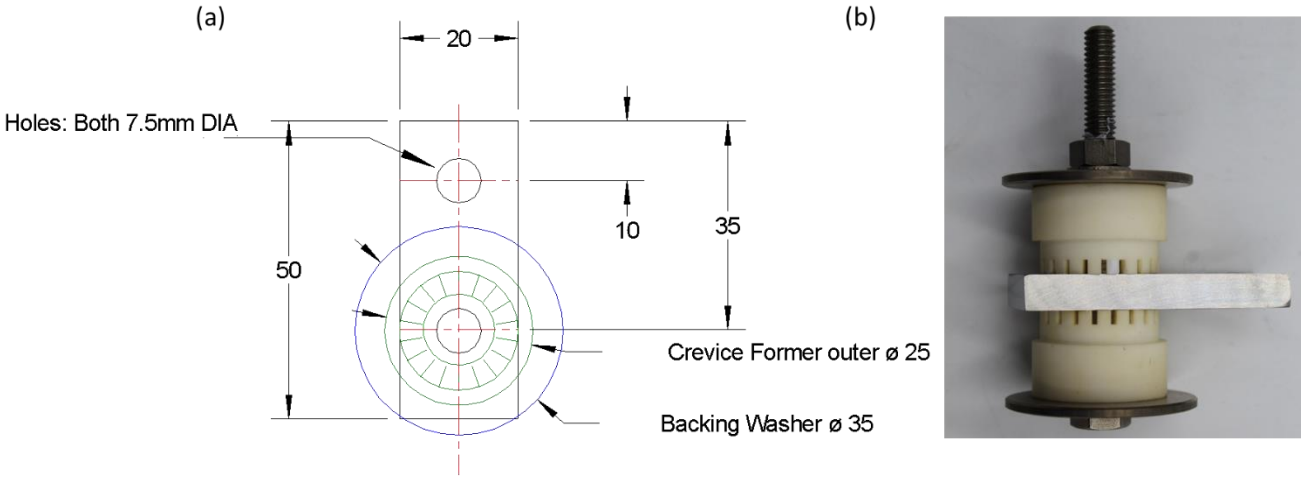

Figure 3 Drawing of crevice corrosion specimens and associated dimensions (a) and photograph of a crevice former assembled on a specimen (b).

4.2.2.2 Stress-corrosion cracking specimens

To evaluate the potential stress corrosion cracking in the materials considered for the heat exchangers, U-bend specimens were also prepared in 316L stainless steel. Space constraints in the autoclaves meant that only one material could be tested, and this material was chosen because it was a relatively cheap heat exchanger candidate material. Following the ASTM G30-97 standard (ref), a rectangular strip was bent at 180^{o} around a predetermined radius and held in place using a Ti grade 2 bolt. The samples were insulated from the bolts and nuts by using ceramic washers and by ensuring the bolt would be secured at the centre of the clearance hole. Figure 4 shows the design of the U-bends and labels the critical dimensions.

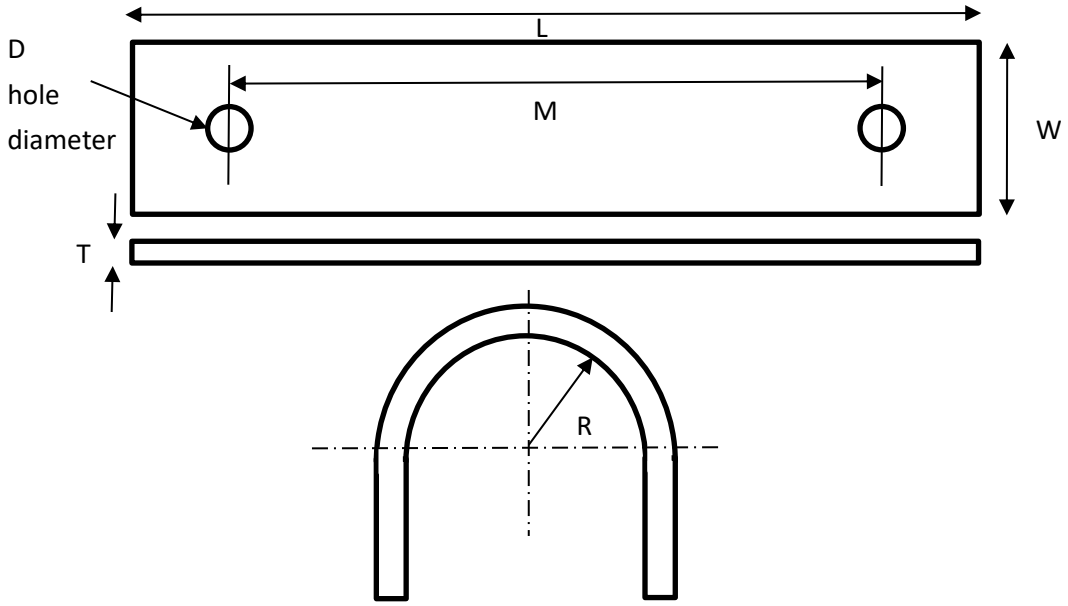

Figure 4 : U-bend dimensions and design

In this work, dimensions were selected as per the following:

Table 6 Dimensions of U-bend specimens

M	150 mm
L	180 mm
T	5 mm
W	20 mm
D	9 mm
R	30 mm

The outer tensile face of each individual U-bend strip was ground to Ra<0.8 µm prior to bending. Roughness was measured using optical profilometry.

4.2.3 Electrochemical testing

4.2.4 Environment and experimental design

4.2.4.1 Brine recipe

The chemistry used in the simulated environment was based on the field conditions that were measured at the Kizildere II geothermal power plant after the low pressure separator, as well as the conditions used as part of D4.2 (Report on formulation of inhibitor against silica scaling, submitted M12) , see Table 7. The solution composition for the tests was chosen to include the elements that would be corrosive to the metals and alloys (chloride), control the pH (DIC), and/or would be involved in the scaling (SiO_2, Ca, Mg).

Zorlu add inhibitor (Kuritherm 4441) to the brine, and so some electrochemical tests were run with this added in order to assess any effect on corrosion behaviour. Tests were deaerated and carried out under 99.998% Ar to simulate the environment after the separator.

Testing temperatures were based on the minimum and maximum operating and design temperatures of the heat exchanger. The maxima were targeted because corrosion processes tend to be accelerated at higher temperatures, but because scaling from certain species is heavier at lower temperatures - which can encourage certain corrosion processes - the minimum temperature was also investigated.

In order to make the solution, the SiO_2 was dissolved into in 0.1M NaOH before being mixed with a solution of $NaHCO_3/Na_2CO_3$. The chloride was then added as $CaCl_2.2H_2O$ and $MgCl_2.6H_2O$.

Table 7. Basis of brine composition for corrosion tests. Items in Bold were employed in the corrosion testing.

Constituent	Brine, mg/l
pH/23°C	**9.77**
SiO_2	**451**
B	24.5
Na	1335
K	156
Ca	**4.75**
Mg	**0.03**
Fe	0.02
Al	0.79
F	27.5
Cl	**111**
CO_2 (=DIC)	**1053**
SO_4	944

4.2.4.2 Tests 1 and 2 – long-term exposure in simulated geothermal brine

Initial tests were designed to evaluate the ability of the selected material to withstand extensive immersion in geothermal brine at elevated temperature. Both Tests 1 and 2 were thus considered in relatively large autoclaves, at both 50°C and 104°C. Both vessels were purged using 99.998% Ar, and tests were conducted at a pressure of 5 barg. Glass liners were used in the autoclaves. Test durations of the tests differed: those tested at 104°C were tested for a longer period of 29 days versus 17 days for those tested at 50°C

Table 8 Samples labelling for exposure tests

Tests	Duration	Substrate \ Tests	Crevice (20x50x5mm)		U-bend	
Test 1- 104°C-static immersion pH 9.7	**29 days**	UNS S32760	1-SDSS-C1	1-SDSS-C2	--	--
		304L	1-304-C1	1-304-C2	--	--
		316L	1-316-C1	1-316-C2	1-316-U1	1-316-U2
		Ti Gr2	1-Ti-C1	1-Ti-C2	--	--
		254SMO	1-254-C1	1-254-C2	--	--
Test 2 - 50 °C-static immersion pH 9.7	**17 days**	UNS S32760	2-SDSS-C1	2-SDSS-C2	--	--
		304L	2-304-C1	2-304-C2	--	--
		316L	2-316-C1	2-316-C2	2-316-U1	2-316-U2
		Ti Gr2	2-Ti-C1	2-Ti-C2	--	--
		254SMO	2-254-C1	2-254-C2	--	--

Table 8 indicates the various samples and material used for the initial autoclave tests in simulated geothermal brine. Each setup is detailed further below.

Test 1 details

Test 1 was performed in the larger autoclave (35L). The sample stand was designed using 4 metallic rods covered in heat shrink, and the 12 samples (10 crevice corrosion samples and 2 U-bends) were installed along these rods. Figure 5 shows photographs of the sample stands.

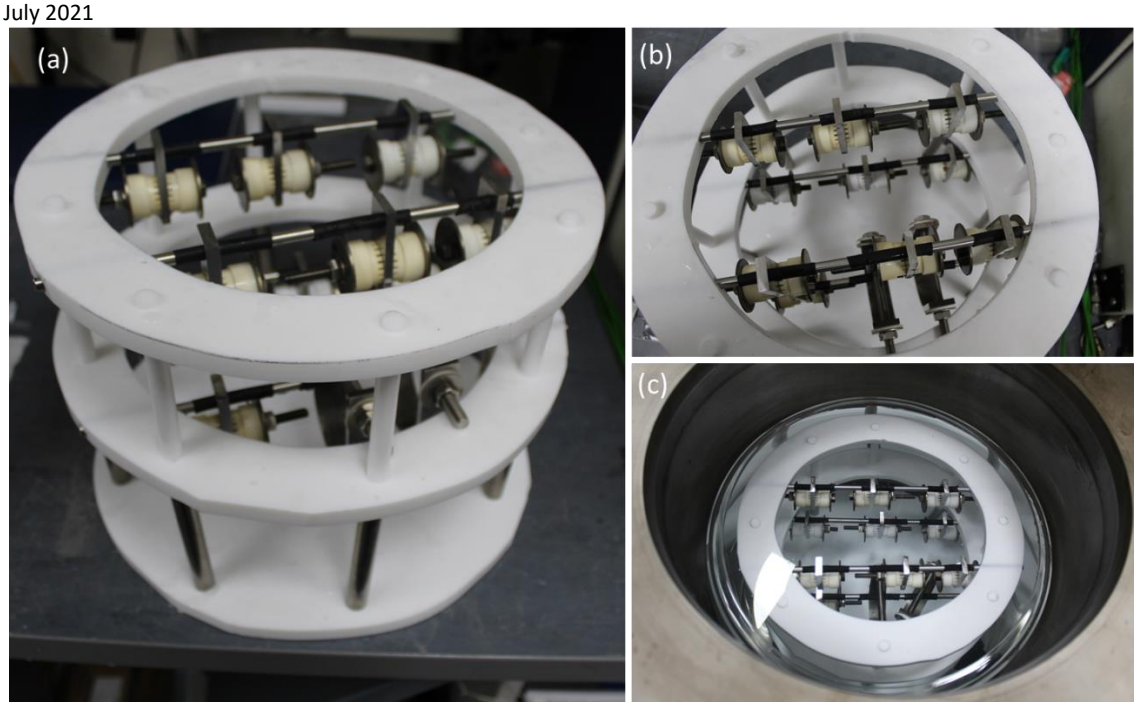

Figure 5: Pictures of sample stand before (a,b) and after insertion in the autoclave (c)

Test 2 details

Test 2 was performed in a smaller autoclave, and samples were thus placed onto a narrower sample tree. Figure 6 shows photographs of the autoclave once sealed as well as the sample tree placed inside the solution.

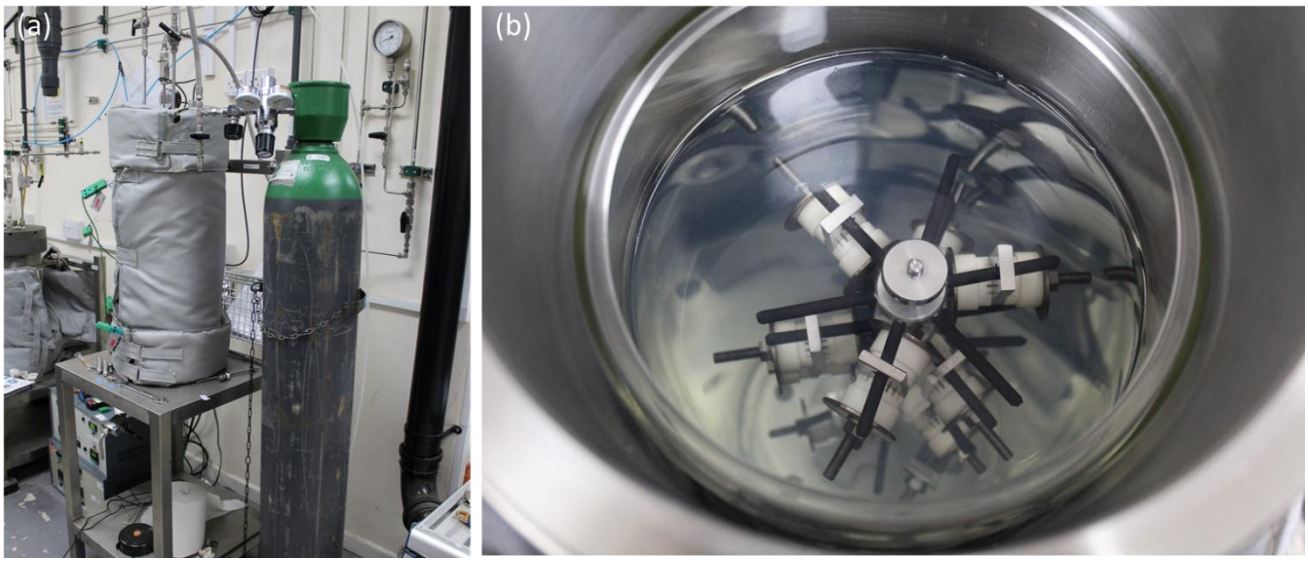

Figure 6: Photographs of the autoclave containing the samples tested at 50°C (a) and the samples on their stand sitting in the autoclave (b)

4.2.4.3 Tests 3 and 4 – potentiodynamic scans

Two of the alloys used for the crevice and U-bend testing were selected for electrochemical testing (Table 9). Ti Gr 1 was chosen as this was felt to be the most likely candidate material for the heat exchanger, from information provided by CEA from the potential manufacturers of the equipment. This alloy is similar in

chemical composition and corrosion performance to Grade 2, which was used for the other corrosion tests (Tests 1 and 2); 304L was selected as a cheaper alternative.

Table 9 Potentiodynamic test specimens

	Tests / Substrate	Pitting (20x20mm exposed area)	
50 °C - pH 9.7 - without inhibitor	304L	PD1-304-P1	PD1-304-P2
	Ti Gr 1	PD1-Ti-P1	PD1-Ti-P2
50 °C - pH 9.7 – with inhibitor	304L	PD2-304-P1	PD2-304-P2
	Ti Gr 1	PD2-Ti-P1	PD2-Ti-P2
120 °C - pH 9.7 - without inhibitor	304L	PD3-304-P1	--

Test 3 Details of tests carried out at 50°C

These tests were carried out in 2 litre glass vessels at ambient pressure at 50°C. A standard 3 electrode cell set-up was used, as shown in Figure 7a. A Ag/AgCl reference electrode was used via a salt bridge, and a Pt/Ti counter electrode was employed. The temperature was regulated by placing the vessels in a water bath (see Figure 7b). The test temperature was controlled to ±1°C. The specimens were held above the solution during the Ar deaeration before being lowered into the deaerated solution to perform the electrochemical testing, which was controlled using an ACM potentiostat. Potential was monitored and allowed to stabilize for at least approximately 6 hours before beginning the potentiodynamic scan at approximately OCP-400mV, then reversed at 5mA/cm^2 . The scan rate was 20mV/min.

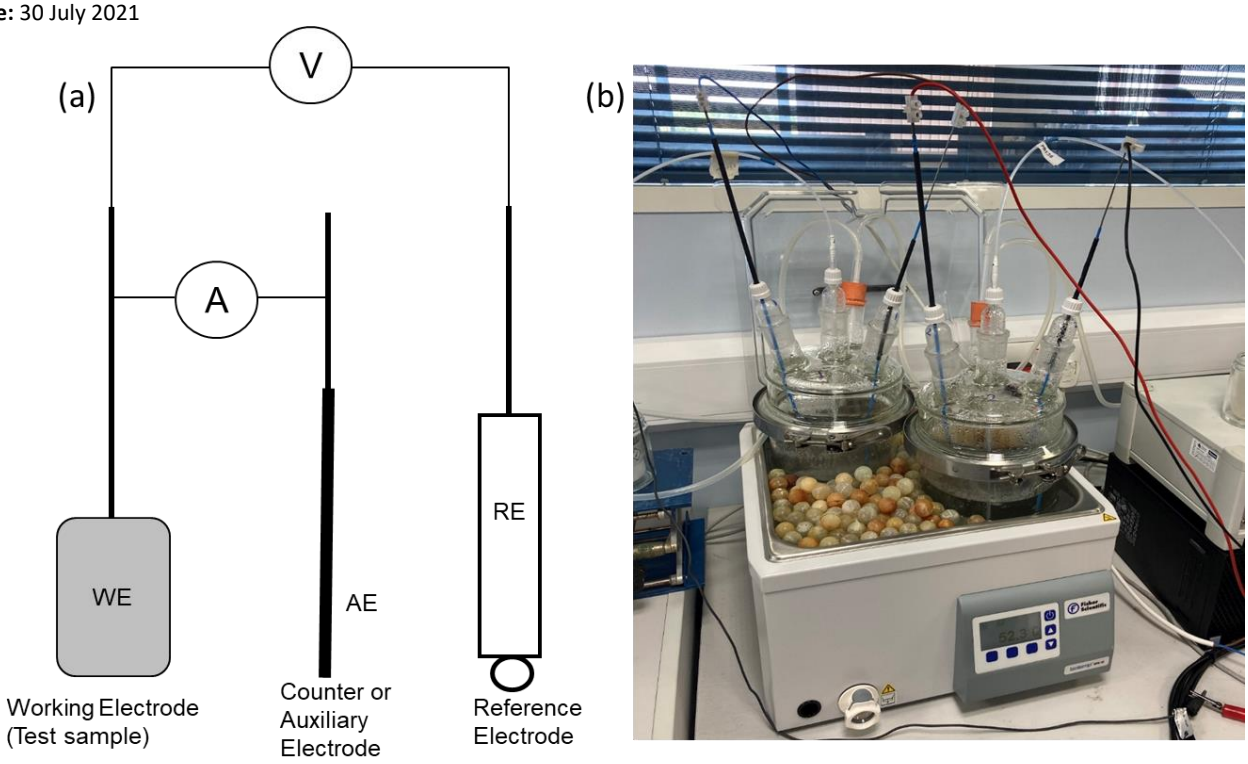

Figure 7 Diagram of the cell (a) and photograph of the testing setup (b)

Test 4 – Details of tests carried out at 120°C

These tests were carried out in an 8.5 litre autoclave at 5barg pressure at 120°C, see Figure 8. The pressure was agreed with Zorlu and the other partners. Similar to the 50°C tests, a standard 3 electrode cell set-up was used. A Pt pseudo-reference electrode and a Pt counter electrode were employed. A polymer reference electrode suitable for high temperatures was purchased for use but following later discussions regarding the pressure, it was decided to not use it for these tests due to safety concerns. The temperature was regulated by a band heater around the metallic Hastelloy C276 autoclave. An additional glass liner vessel was used to contain the test solution and test electrodes to help ensure electrical isolation to the metallic vessel. The test temperature was controlled. The specimen was held in the solution during the Ar deaeration for a period of 24hrs prior to heating and electrochemical testing using an ACM potentiostat. The system was monitored and allowed to stabilize overnight before beginning the potentiodynamic scan.

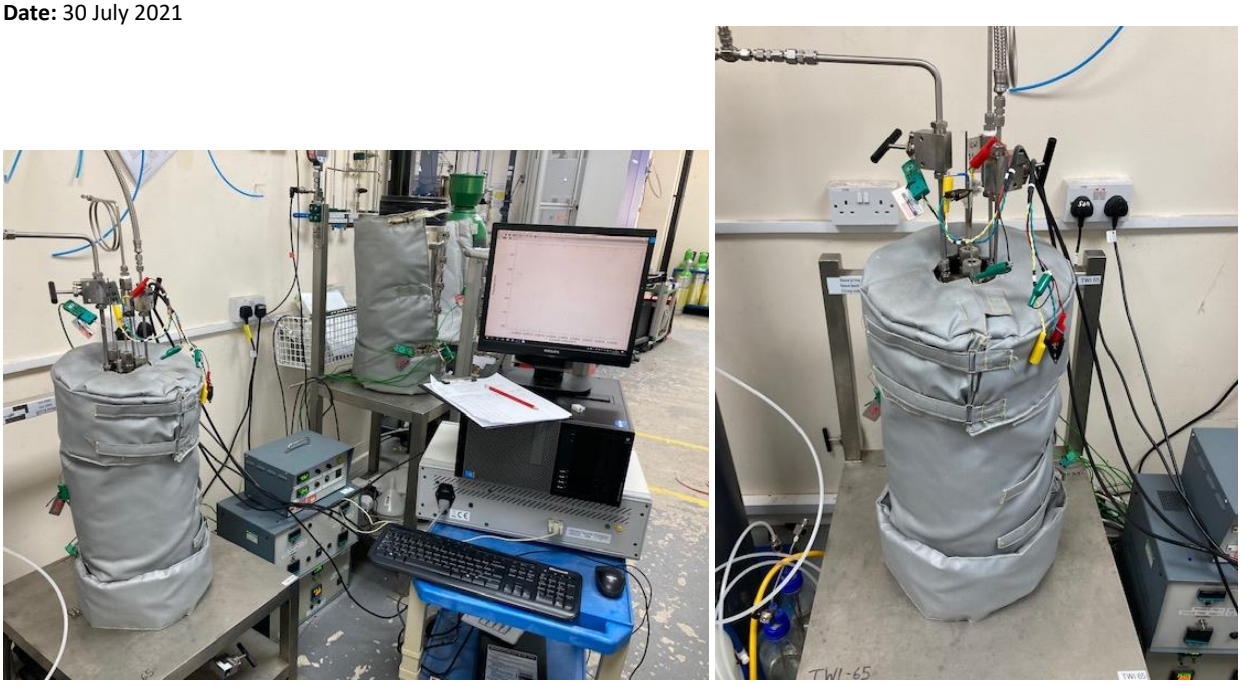

Figure 8 Photographs of the 120°C electrochemical testing setup

4.2.5 Post-test characterisation

4.2.5.1 Visual examination

Specimens were visually examined before and after testing. Photographs were taken to record observations.

4.2.5.2 Mass loss

The crevice corrosion specimens (without crevice formers) and U-bend specimens (with bolts) were weighed before and after testing in order to evaluate the extent of any corrosion. Specimens were not cleaned before weighing after test in order to evaluate the extent of scaling.

4.2.5.3 Optical profilometry

The topography of the samples was characterised using the Alicona InfiniteFocusSL (Bruker, Austria). Through non-contact 3D optical measurement, a surface of approximately 5x10 mm was characterized on each selected coupon, using a 20x objective corresponding to a vertical resolution of 100 nm. These measurements aimed to quantify the depth of crevice corrosion on 304L crevice corrosion samples.Non-destructive testing

Dye penetrant testing was carried out on the tensile face of the U-bend samples in order to look for cracking. Photographs were taken to record observations.

4.2.5.4 Scanning electron microscopy (SEM)

SEM and EDX (energy dispersive X-ray spectroscopy) were used to examine one of each of the duplicates of long-term crevice corrosion specimens after testing. The most corroded/scaled specimens were selected visually for this examination.

The short-term potentiodynamic scan samples tested at 50°C without inhibitor were also examined in the SEM for evidence of scaling; these specimens were considered to be of most risk of scaling.

4.3 Chemical compatibility results

4.3.1 Crevice corrosion

Table 10 Results of crevice corrosion tests

Conditions	Sample label	Weight loss (-) /gain (+), g	Number of crevice sites attacked (#/40)
104° C, 29 days	1-SDSS-C1	0.0075	0
	1-SDSS-C2	0.0099	0
	1-316-C1	0.0042	0
	1-316-C2	0.0259	0
	1-254-C1	0.0158	0
	1-254-C2	0.0018	0
	1-304-C1	0.0119	0
	1-304-C2	0.0544	0
	1-Ti-C1	0.0311	0
	1-Ti-C2	0.0068	0
50 ° C, 17 days	2-SDSS-C1	0.0002	0
	2-SDSS-C2	0.0402	0
	2-316-C1	0.0258	0
	2-316-C2	0.0115	0
	2-254-C1	0.0203	0
	2-254-C2	0.0131	0
	2-304-C1	-0.0105	0
	2-304-C2	0.037	0
	2-Ti-C1	0.0056	0
	2-Ti-C2	0.0098	0

Table 10 shows the weight loss measurements - after removal of the crevice formers – which mostly showed weight gain. This correlated with the visual observations of scaling of the samples in both tests. The results of the further post-test evaluations are shown in Appendix A. These confirmed the presence of silica scale on all of the specimens examined, and also the presence of calcium and magnesium-rich scaling. The scale was visible on all parts of the samples, including underneath the crevice formers.

There was also one recorded weight loss. Further examination of this specimen confirmed the presence of small corrosion pits on the surface, which were not restricted to the regions beneath the crevice formers. Alicona analysis showed that the depth of these pits was up to approximately 25 microns.

4.3.2 U-bends

The DPI results of the U-bend testing confirmed that no cracking was observed. Weight loss measurements – with the bolts attached – showed weight gain, see Table 11. The tests at the lower test temperature of 50°C clearly exhibited higher weight gain, consistent with silica scaling being more prevalent at lower temperatures.

Table 11 Results of U-bend tests

Conditions	Sample label	Weight gain, g	Cracks
104 deg C	1-316-U1	0.0031	None
	1-316-U2	0.0029	None
50 deg C	2-316-U1	0.2004	None
	2-316-U2	0.1646	None

The results of the post-test evaluations are shown in Appendix B.

4.3.3 Potentiodynamic scans

Potentiodynamic scans were conducted on 304L and Ti specimens. Figure 9 shows the typical curves obtained following these scans, providing information of the surface corrosion of the scanned specimens. Potential drives the reaction at the anode or cathode, shown as changes in current density. Values such as Breakdown potential and Corrosion potential were measured and recorded. Cyclic polarisation scans were conducted throughout this section, meaning that voltage was increased at a certain scan rate to a certain value, and then reversed back to the Corrosion potential.

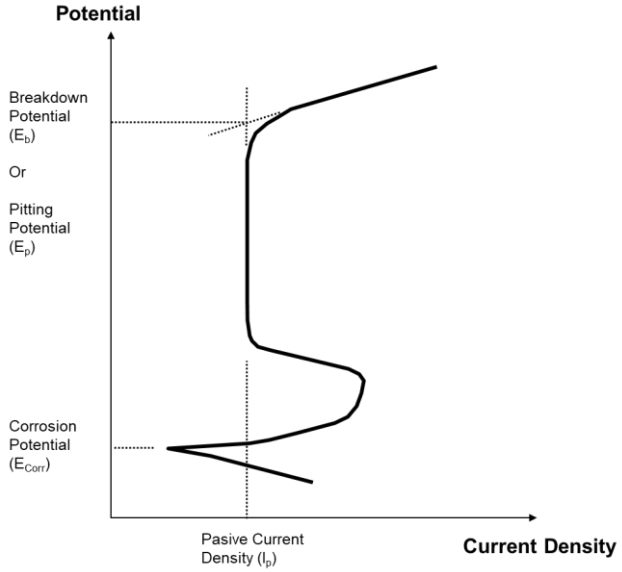

Figure 9 Typical potential/current curve obtained following potentiodynamic scans.

Figures 10-14 show the results of the 304L and Ti specimens tested at 50°C without and with inhibitor, and the specimens tested at 120°C without inhibitor. The duplicate tests displayed good agreement in values of rest potential (E_{corr}), breakdown potential (E_p), repassivation potential (E_{RP}) and passive current (i_P) range, see Table 12. The materials exhibited passive behaviour (low passive current) in the simulated geothermal brine under all test conditions.

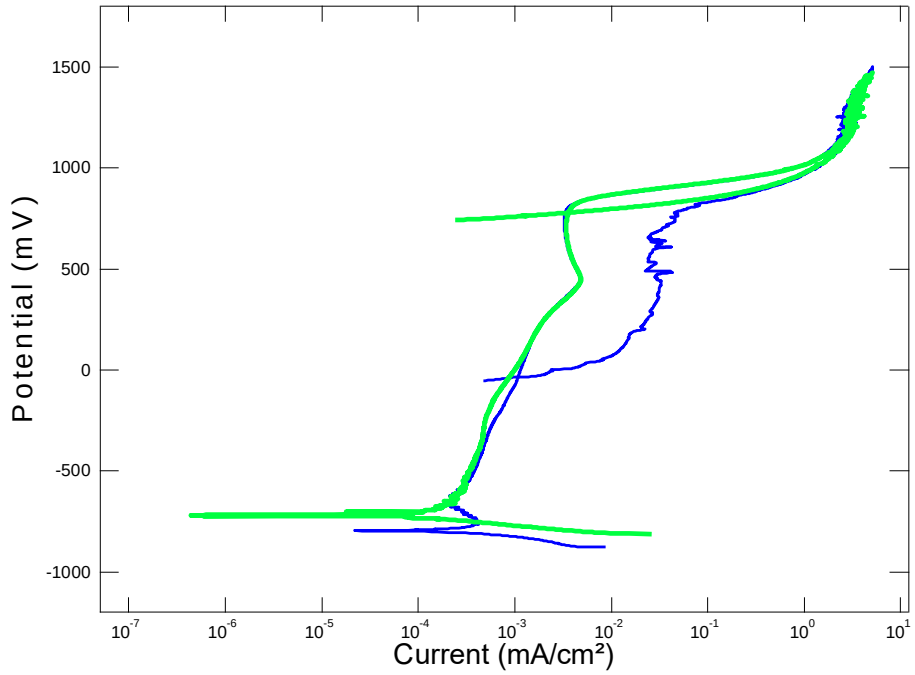

Figure 10 304L tested at 50°C without inhibitor, pH 9.7 (Potential vs. Ag/AgCl)

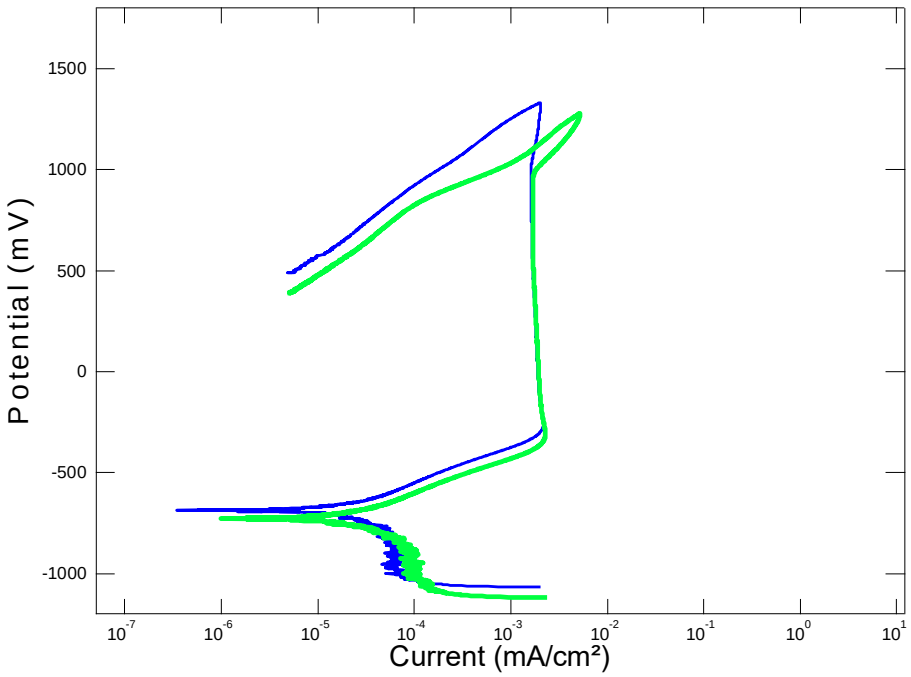

Figure 11 Titanium Gr 1 tested at 50°C without inhibitor, pH 9.7 (Potential vs Ag/AgCl)

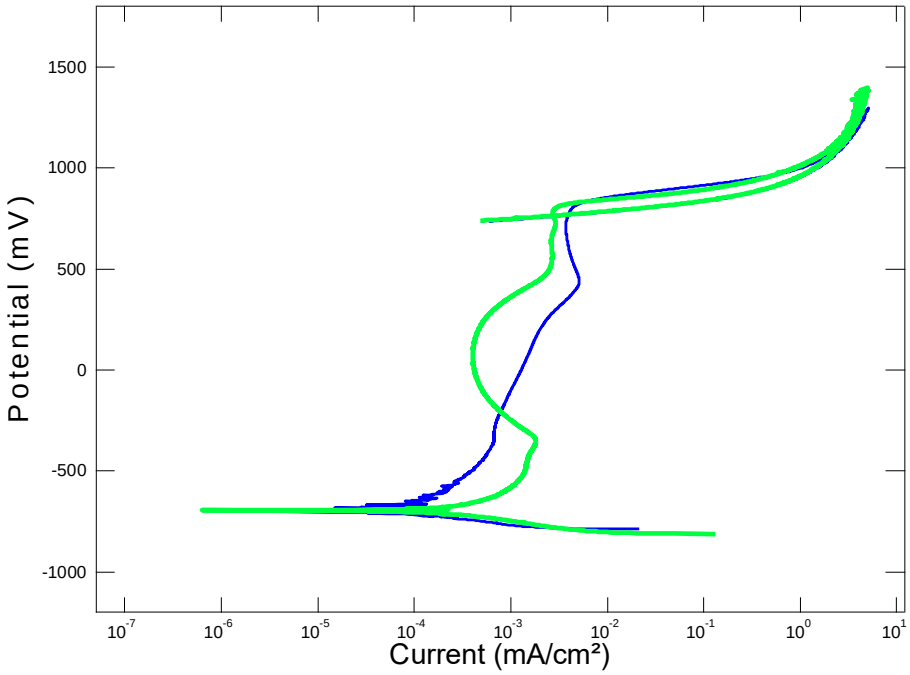

Figure 12 304L tested at 50°C with inhibitor, pH 9.7 (Potential vs Ag/AgCl)

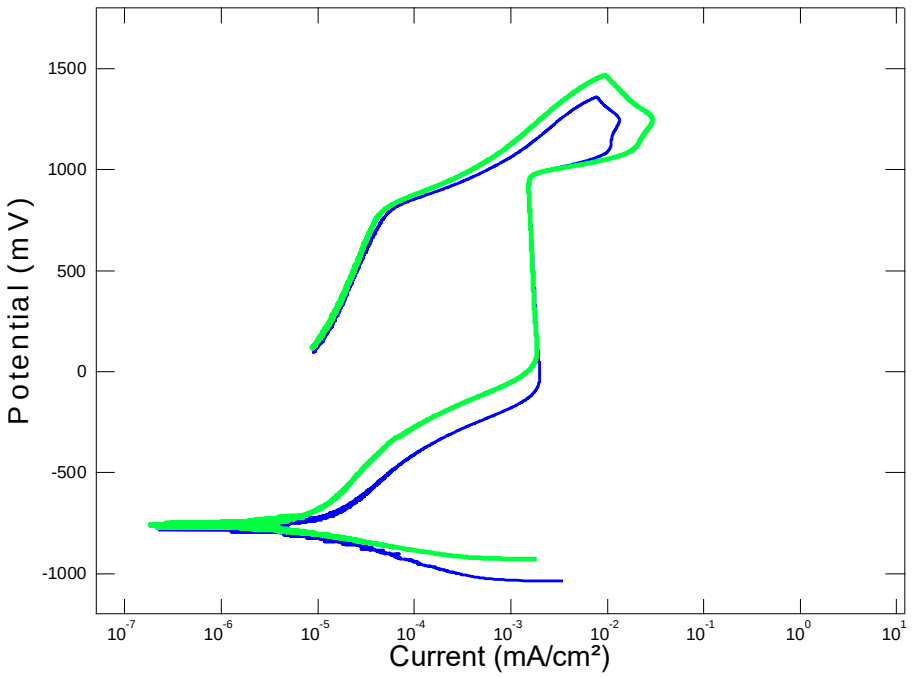

Figure 13 Titanium Gr 1 tested at 50°C with inhibitor, pH 9.7 (Potential vs Ag/AgCl)

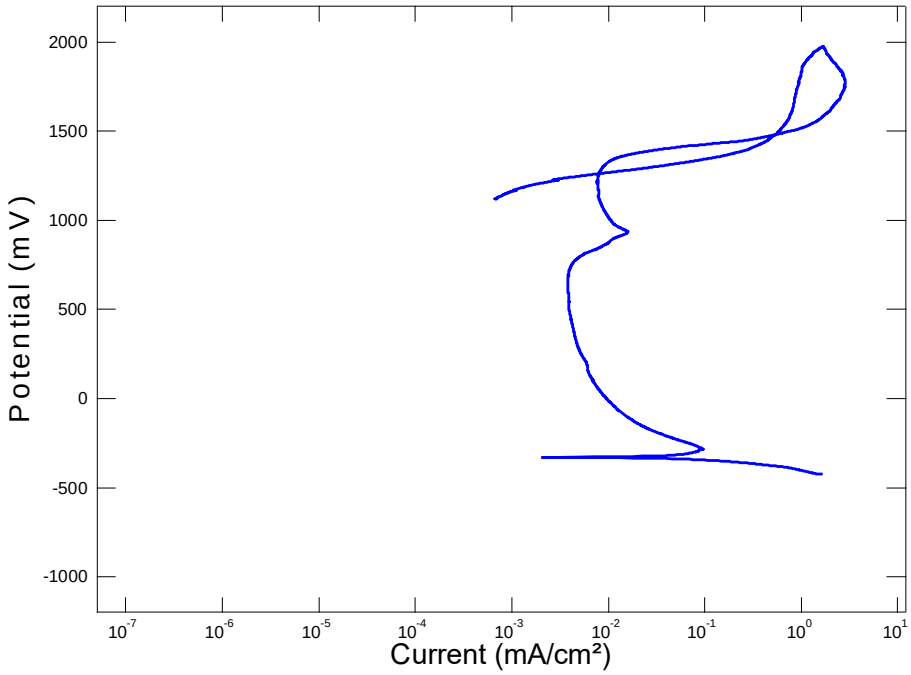

Figure 14 304L tested at 120°C without inhibitor, pH 9.7 (Potential vs Pt)

Table 12 Selected parameters measured during potentiodynamic scans. NA = not applicable.

	Substrate / Tests	Pitting (20x20mm exposed area)	E_{corr} (mV vs Ag/AgCl)	E_p (mV vs Ag/AgCl)	E_{rp} (mV vs Ag/AgCl)	I_p range (mA/cm^2)	Ep – Erp (mV)
50 °C - pH 9.7 - without inhibitor	304L	PD1-304-P1	-799	793	-33	2.2E-4-4.7E-3	825
		PD1-304-P2	-721	826	774	2.9E-4-4.9E-3	52
	Ti Gr 1	PD1-Ti-P1	-693	1003	NA	1.6E-3-1.9E-3	NA
		PD1-Ti-P2	-725	982	NA	1.7E-3-2.3E-3	NA
50 °C - pH 9.7 – with inhibitor	304L	PD2-304-P1	-703	826	726	6.7E-4-4.2E-3	100
		PD2-304-P2	-697	812	756	4.2E-4-2.9E-3	56
	Ti Gr 1	PD2-Ti-P1	-778	966	NA	1.6E-3-2.0E-3	NA
		PD2-Ti-P2	-758	966	NA	1.6E-3-1.9E-3	NA
120 °C - pH 9.7 - without inhibitor	304	PD3-304-P1	-332 (*)	1315 (*)	1261 (*)	4.0E-3-1.6E-2	56

(*) potential vs Pt electrode

The results of the post-test evaluations on the specimens tested at 50°C without inhibitor are shown in Appendix C.

4.4 Conclusions of corrosion testing

The results from the short-term potentiodynamic testing indicated that both 304L and Ti Gr 1 were passive in the simulated geothermal brine. No pitting or crevicing behaviour was observed from electrochemical scans and this was confirmed from post-test examination of the samples.

The results from the short-term potentiodynamic testing indicated that the effect of the inhibitor on the corrosion behaviour was minimal. However some differences in the cathodic reverse scan for the Ti alloy was observed, possible due to the inhibitor affecting the scaling behaviour.

The results from the long-term SCC testing indicated that 316L was resistant to SCC in the simulated geothermal brine.

The results from the long-term crevice corrosion testing indicated that all alloys were resistant to crevice corrosion in the simulated geothermal brine. However, some small corrosion pits were observed on the 304L specimens.

5. FOULING DETECTION

In the field of fouling detection, three conventional methods can be identified:

- Infrared thermography: qualitative method (significant sources of error) to locate the fouling problem,
- Visual inspection: detect the level of fouling through the user experience: subjective information,
- Direct measurements at the heat exchanger terminals: inlet and outlet temperatures and flow measurements to verify the overall efficiency of the heat exchanger.

The solution adapted to Kizildere ZII is fouling measurement by pressure and temperature differences measurement.

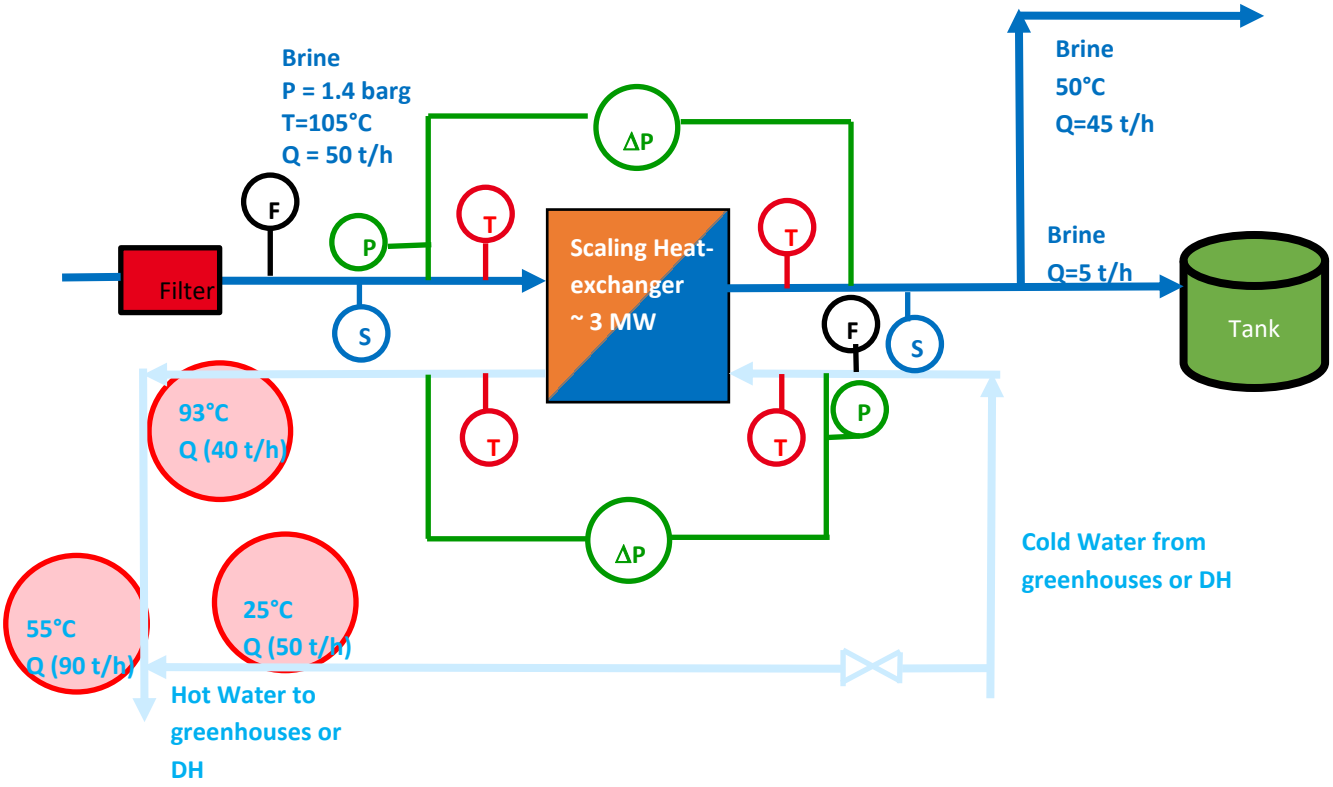

T : Temperature probes (preferably platinum sensors)

P / ΔP : Pressure and differential pressure sensors

F : Flow meter (electromagnetic flow meter)

S : Samples (for further composition analysis)

Figure 15: Simplified PI&D of scaling detection system

Thermal power is evaluated by the following equation:

$$\mathcal{P} = \rho Q_V C_p \Delta T$$

With ρ density (kg·m^{-3}), Q_V volumetric flow rate (m^3·s^{-1}) and C_p, fluid specific heat (J·kg^{-1}·K^{-1}).

The temperature difference of the fluid (hot or cold) between the inlet and outlet of the exchanger is noted ΔT (K).

Global heat transfer coefficient *U* ($W \cdot m^{-2} \cdot K^{-1}$) is can be calculated from the average power exchanged using the equation:

$$U = \frac{\mathcal{P}}{S \Delta T_{ML}}$$

S (m^2) is the area available for heat transfer in the HX and ΔTML is the logarithmic mean temperature difference (K). For a countercurrent exchanger, it is calculated according to equation below:

$$\Delta T_{ML} = \frac{(T_{I,H} - T_{O,C}) - (T_{O,H} - T_{I,C})}{ln\left(\frac{T_{I,H} - T_{O,C}}{T_{O,H} - T_{I,C}}\right)}$$

The temperature is noted T (K). The subscripts *I* and *O* refer to the inlet and outlet respectively, while *H* and *C* refer to the hot and cold fluid in the HX.

The fouling resistance (denoted Rf, in $m^2 \cdot K \cdot W^{-1}$) is the additional thermal resistance created by the fouling deposit on the heat exchanger surfaces. It is calculated as follows:

$$R_f(t) = \frac{1}{U(t)} - \frac{1}{U_0}$$

U(t) and U_0 are the overall heat transfer coefficients of the HX at the time of measurement and at the start of the test respectively (nominal values).

To accurately estimate fouling resistance, we can do the calculation on the primary and/or secondary side.

The pressure between inlet and outlet will be regularly measured. When fouling develops, the average surface area of a flow channel decreases leading to a pressure drop at constant flow rate. This method is standard and can be used as input for other methods like temperature measurements or additional sample collection as suggested by the project partners.

6. PRE SIZING AND CHARACTERISTICS OF THE HEAT EXCHANGER

The CEA's approach is to work with leaders in plate heat exchangers and seek to optimise the design according to the sizing data, and low deposition criteria such as residence time to be minimised.

Here is a list of manufacturers who can correspond:

- BARRIQUAND (not a gasket specialist)
- KELVION
- KAPP (only reseller)
- SWEP
- ALFA LAVAL

Among all the suppliers, the CEA considers that Alfa Laval is particularly competent in the manufacturing of plate and gasket heat exchangers applied to geothermal field. CEA therefore consulted this manufacturer for the pre design of the HX.

The manufacturer alerts to the importance of knowing the chloride rate in order to choose the alloy of the exchanger. A too high chloride rate is not compatible with stainless steel and makes us switch to titanium heat exchangers.

For instance, for a pH of seven, the average rates are:

- Stainless steel: 20 ppm
- Alfalaval alloy: 1000 ppm
- Titanium: 10 000 ppm

The proposed assembling mode is a **Plate and Gasket HX** with Titanium and HNBR (high temperature nitrile) clip-on gaskets. The heat load is 3MW.

The characteristics are as follow:

- Stamping depth 4mm (filtration required 1,2mm or 1mm),
- New distribution to limit the dead zones which are the starting points of fouling,
- High turbulence, therefore much less sensitive than tubular exchangers to fouling,
- 15% thermal margin to fight against fouling,
- Identical plates, therefore stacking of plates easy to put back after opening.

The proposed exchanger includes a **new-patented plate** design specially designed to limit scaling (cf. Figure 16). According to the manufacturer, this exchanger ensures a good distribution, favors turbulence and limits scaling. The clip-on seals allow dismantling for easy maintenance and have a service life of 10 years without opening the exchanger and 7 years if opened.

The manufacturer, taking into account the physical properties of the brine (cf. Table 13), proposes Titanium plates and a cleaning every 6 months for the turbulent plate heat exchanger.

Table 13 Kizildere II Brine Composition (mg/L) [7]

K	**Na**	**Ca**	**Mg**	**Li**	**PO_4**	**Hg**	**Sr**	**Zn**	**Ba**	**Al**
196,00	1538,00	3,87	0,23	5,40	<0,05	<0,005	0,10	<0,05	<0,05	1,30
Fe	**B**	**SiO_2**	**NH_4+**	**CO_3 2-**	**HCO_3-**	**Cl-**	**SO_4 2-**	**F -**	**Br -**	**As**
<0,05	24,00	460,00	8,00	127,00	2390,00	175,00	937,00	28,00	0,50	0,97

Alfa Laval has proposed two designs with co and counter current flows (cf. Table 14). CEA will ask the manufacturer for an off-nominal calculation so that the fluid can exit hotter (70°C for example). The co-current configuration may be more interesting in the present case because it is possible to decrease the wall temperature by co-current configuration. It will affect the price, as more surface area is required with co-current configuration.

Table 14 Pre design of the HX from Alfalaval

Items	Units	Co-Current HX	Counter-Current HX
HXs type		Plate	Plate
Technology options		Plate & gaskets	Plate & gaskets
Plate Material type/ Thickness	**/[mm]**	Titanium/0.6	Titanium/0.6
Number of plates		89	60
Gasket material and fixing		NBRP ClipGrip™	NBRP ClipGrip™
Extension capacity		5 plates	12 plates
Unit dimension	**[mm]**	860 x 480 x 1050	640 x 480 x 1050
Inlet Temperature	**[^{0}C]**	104/25 (brine/water)	104/25 (brine/water)
Outlet temperature	**[^{0}C]**	55/50 (brine/water)	50/55 (brine/water)
Pressure drop	**[kPa]**	12.8/26.9 (brine/water)	28/42.5 (brine/water)
Power	**[kW]**	2849	3139
ΔTLM		26.8	35.7
Overall heat transfer coefficient	**[W m^{-2} K^{-1}]**	4887	6071
Exchanged surface	**[m^2]**	21.75	14.5
Service margin	**%**	20.2	15.3
Operating pressure	**[bar]**	10/10 (brine/water)	10/10 (brine/water)
Test pressure (hydraulic test pressure, about 1.5 x the working pressure which itself is higher than the operating pressure)		14.3/14.3 (brine/water)	14.3/14.3 (brine/water)
Fluid flow rates	**[kg/h]**	50 000(brine) 98 212 (water)	50 000(brine) 90 184 (water)

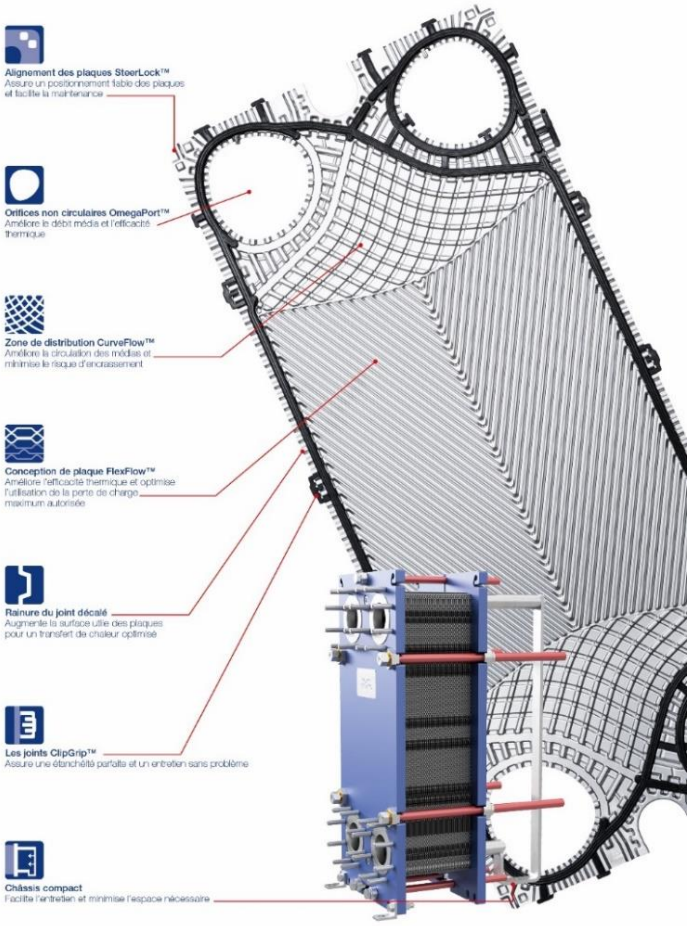

SteerLock™ Plate alignment: Ensures reliable plate positioning and facilitates maintenance

Omegaport™ non-circular ports: Improves media flow and thermal efficiency

Distribution area CurveFlow™: Improves media circulation and minimises the risk of clogging

FlexFLow™ plate design: Improves thermal efficiency and optimises the use of the maximum allowable pressure drop

Offset joint groove: increases the effective surface area of the plates for optimum heat transfer

ClipGrid™ gaskets: ensure a perfect seal and trouble-free maintenance

Compact chassis: facilitates maintenance and minimises space requirements

Figure 16: T type heat exchanger from Alfa Laval

Kelvion has proposed three different designs with counter current flows. We compared the two closest designs offered by the two manufacturers in the following table:

Table 15 Pre design of the HX from Kelvion and Alfalaval

Items	Units	Counter-Current HX Kelvion	Counter-Current HX Alfalaval
HXs type		Plate	Plate
Technology options		Plate & gaskets	Plate & gaskets
Plate Material type/ Thickness	**/[mm]**	Titanium/0.5	Titanium/0.6
Number of plates		60	60
Gasket material and fixing		NBR Clipped on	NBRP ClipGrip™
Extension capacity		NC	12 plates
Unit dimension	**[mm]**	835 x 524 x 1110	640 x 480 x 1050
Inlet Temperature	**[^{0}C]**	105/20 (brine/water)	104/25 (brine/water)
Outlet temperature	**[^{0}C]**	50/55 (brine/water)	50/55 (brine/water)
Pressure drop	**[kPa]**	11.5/19.7 (brine/water)	28/42.5 (brine/water)
Power	**[kW]**	3000	3139
ΔTLM		39.15	35.7
Overall heat transfer coefficient	**[W m^{-2} K^{-1}]**	NC	6071
Exchanged surface	**[m^2]**	15.66	14.5
Service margin	**%**	14.83	15.3
Operating pressure	**[barg]**	10/10 (brine/water)	9/9 (brine/water)
Test pressure (hydraulic test pressure, about 1.5 x the working pressure which itself is higher than the operating pressure)	**[barg]**	13/13 (brine/water)	13.3/13.3 (brine/water)
Fluid flow rates	**[kg/h]**	59 368 (brine) 73 830 (water)	50 000 (brine) 90 184 (water)

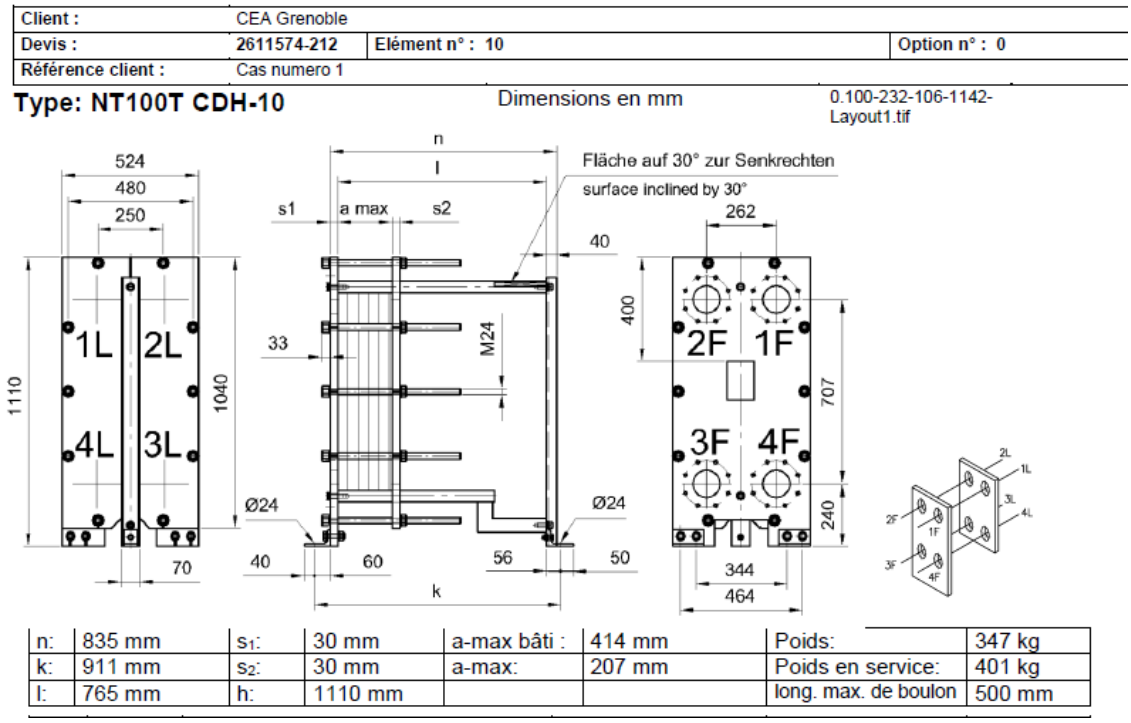

Figure 17: Dimensional drawing of the Kelvion HX

7. DATA OVERVIEW FINAL DESIGN

The next step was to initiate a tender bid with a few manufacturers, as CEA is conducted by the directive of public market for the building of the device. The device will be ordered after receiving their bid and quotation.

The tender has been launched and the answers from manufacturers are expected mid-July.

So far, Kelvion has proposed a design as shown in Table 15 Alfalaval will send an updated design certainly close to the pre design proposed in Table 14. Barriquand and Kapp were not selected as they were not gasket specialists or only resellers. SWEP has declined because they could not make a removable HX.

8. CONCLUSIONS

One heat exchangers will be manufactured, fed with brine on hot side and water on cold side.

Plate & gasket technology with clipped-on gaskets to open the HX is the best option to contribute to an innovative aspect of the project. Pre sizing calculations have been achieved to evaluate the feasibility of such design.

To prevent scaling, different solutions can be proposed:

- Chemical: pH modification, additional chemical inhibitors
- Thermal : reduction of resident time and turbulence enhancement, eventually decreasing of the wall temperature
- Protection the HX with an external filter
- Perform preventive maintenance without opening, by chemical circulation
- Cleaning frequency: manufacturer recommends every 6 months for the following brine composition on Kizildere II site, with sensors for performance monitoring.
- Monitor the operating parameters $\Delta P/\Delta T$ to assess the fouling rate

CEA will implement the last option with a suitable instrumentation to detect fouling.

To conclude, the provisional schedule for the manufacture and delivery of the HX (cf. Table 16) is presented:

Table 16 Provisional timetable for the supply of the HX

Task	18 June	19 July	20 Aug	21 Sep	22 Oct	23 Nov	24 Dec	25 Jan	26 Feb
Consolidation of specifications									
Final design HX									
Order HX and instrumentation									
Manufacture									
Shipping time + Sending to KZII									
Deliverables		D4.3							D4.6

9. REFERENCES

[1] Pillai V, Kale N, Holmes B, Sabard A, Alp Sahiller H, Halacoglu U, Rouge S, Baker D, Updated End User spec & document agreed with users, including KPI for two case study sites, Geosmart - Technologies for geothermal to enhance competitiveness in smart and flexible operation, D1.8, 2021.

[2] Nogara J, Zarrouk SJ, 2018: 'Corrosion in geothermal environment Part 2: Metals and Alloys, Renewable and Sustainable Energy Reviews, Vol.82, pp.1347-1363.

[3] P. Ellis and M. Conover, "Materials selection guidelines for geothermal energy utilisation system," NASA STI/Recon, 1981.

[4] P Ellis, Companion Study Guide to Short course on geothermal corrosion and mitigation in low temperature geothermal heating systems, DCN 85-212-040-01, 1985.

[5] Kurata Y, Sanada N, Nanjo H, Ikeuchi J, 1992: 'Material Damages in Geothermal Power Plants', Proc. 14th New Zealand Geothermal Workshop 1992, pp.159-164.

[6] Şengün R, Halaçoğlu U, 2019: 'KIZILDERE GEOTHERMAL FIELD GEOCHEMISTRY REPORT', Geosmart,

[7] Alp Sahiller H., Rougé S. Enhancing the flexibility of electricity generation and heating for Kızıldere II geothermal power plant by demonstrating heat storage systems. 9th Eur. Conf. Ren. Energy Sys. 21-23 April 2021, Istanbul, Turkey

Appendix A

Results sheets for crevice corrosion specimens

Specimen identity :	1-254-C1
Test temperature:	104^{o}C
Photograph before	Photographs after

Specimen identity :	1-254-C2
Test temperature:	104°C
Photographs before	Photographs after
	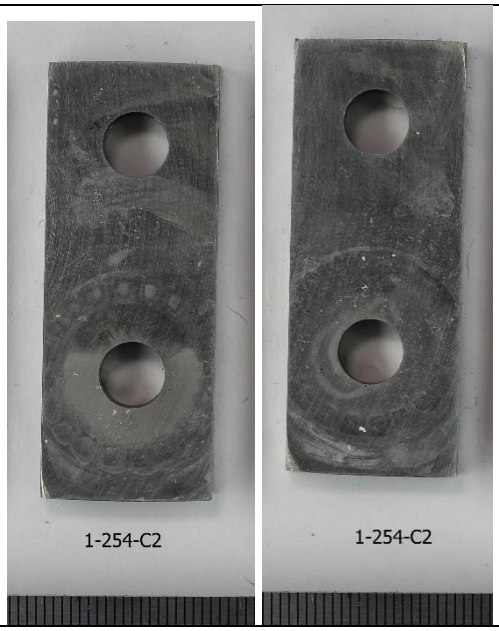
SEM images after	EDX analysis after
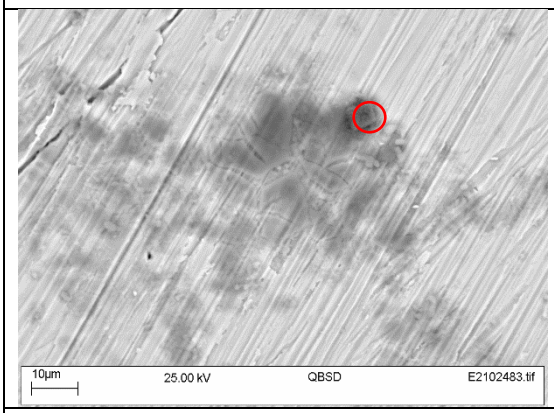	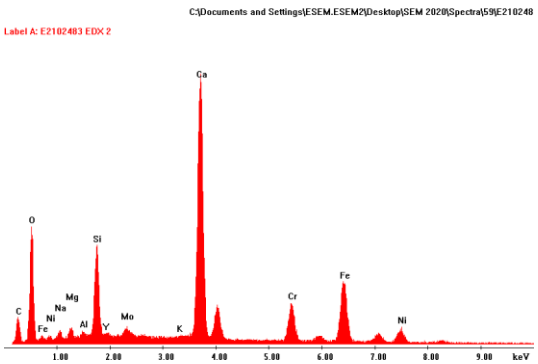
Scale	Evidence for silica scale and scale containing magnesium and calcium

Specimen identity :	2-254-C1
Test temperature:	50^{o}C
Photographs before	Photographs after
SEM images after	EDX analysis after
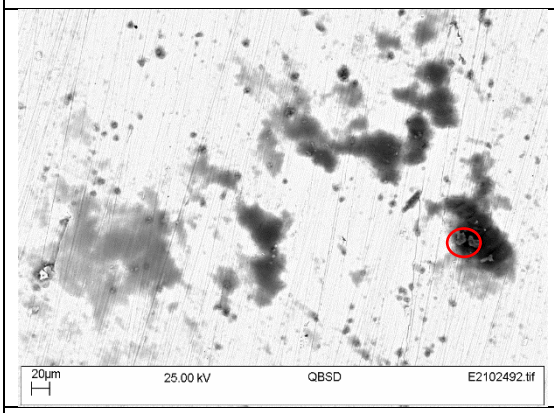	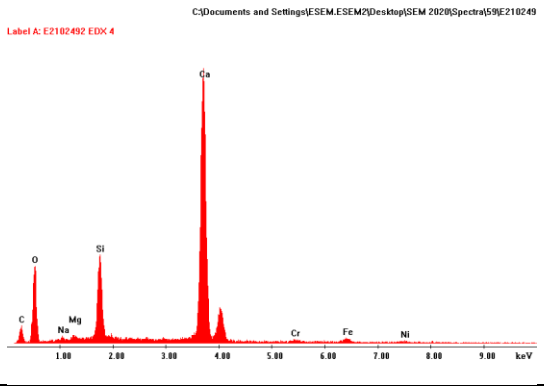
Red circle denotes approximate position of EDX analysis	
Scale	EDX evidence for silica and magnesium-rich scale

Specimen identity :	2-254-C2
Test temperature:	50^{o}C
Photographs before	Photographs after

Specimen identity :	1-304-C1
Test temperature:	104°C
Photographs before	Photographs after
	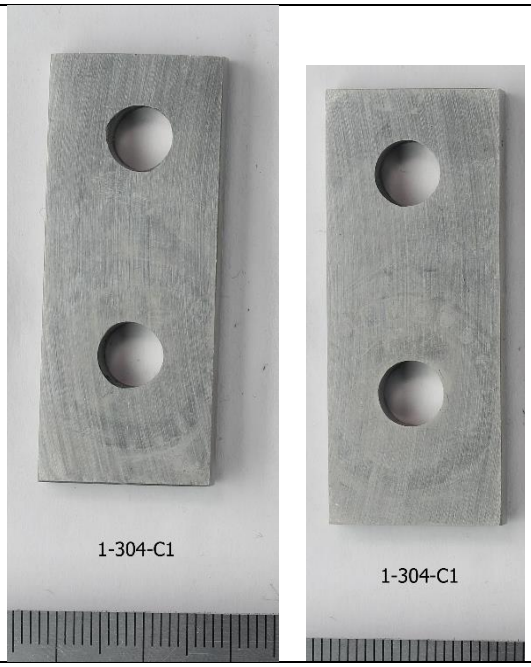
Alicona surface profiling area 1	Alicona surface profiling area 2
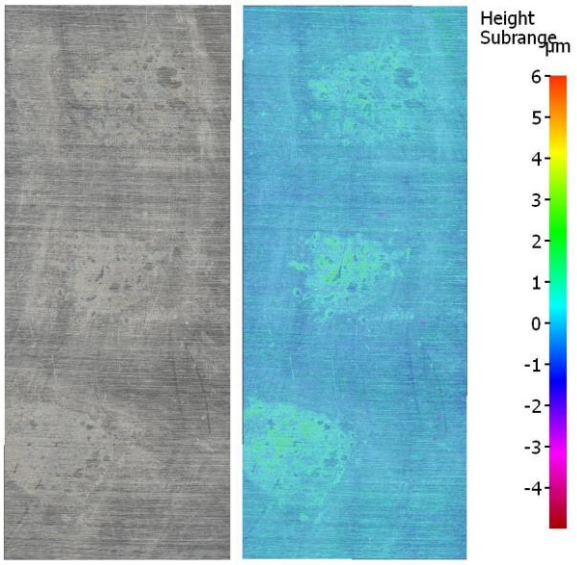	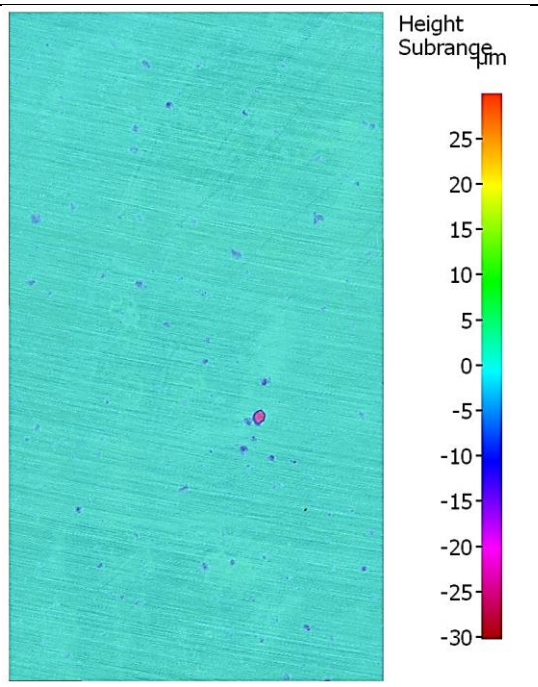

Specimen identity :	1-304-C2
Test temperature:	104°C
Photographs before	Photographs after
	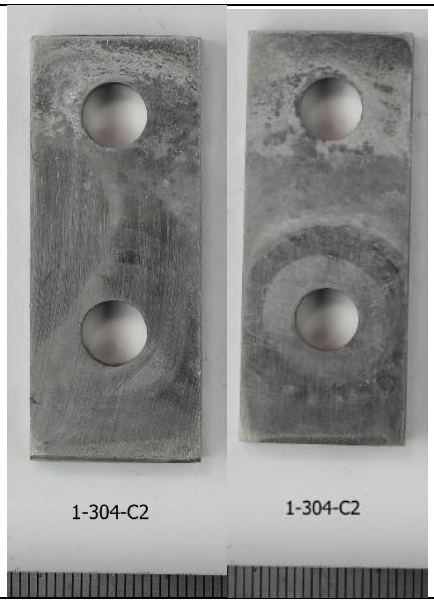
SEM images after	EDX analysis after
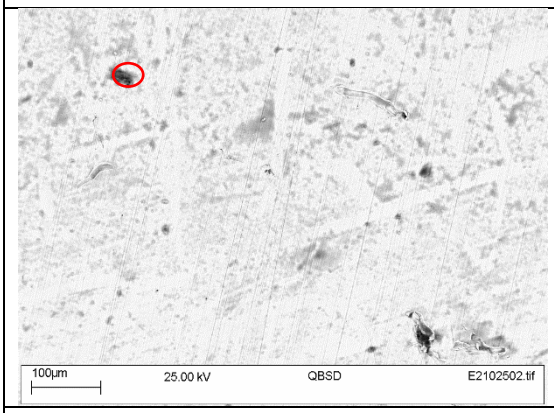	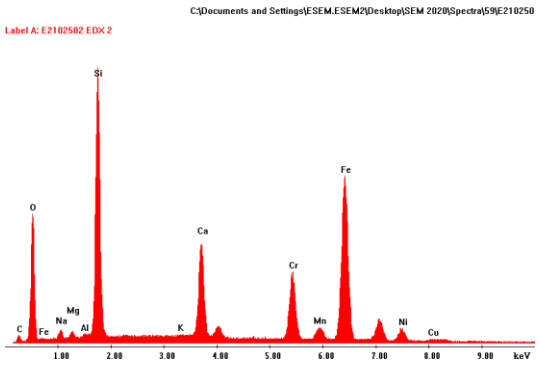
Red circle denotes approximate position of EDX analysis	
Scale	Evidence for silica, and calcium-rich scale
Alicona surface profiling	
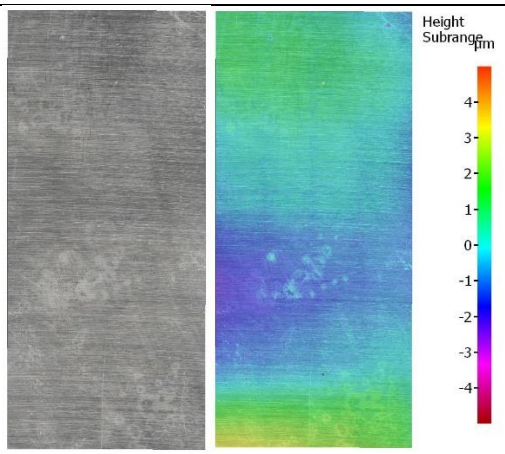	

Specimen identity :	2-304-C1
Test temperature:	50^{o}C
Photographs before	Photographs after
SEM images after	EDX analysis after
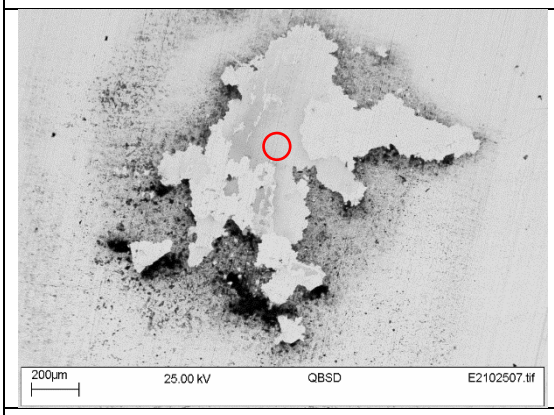	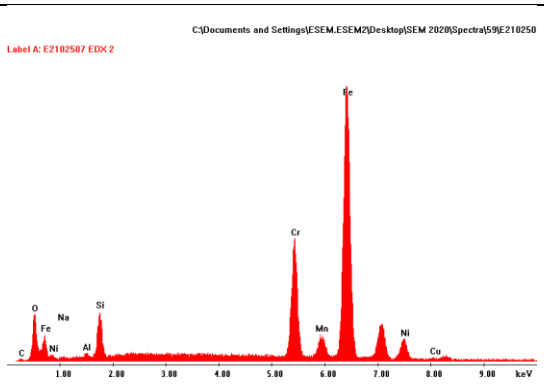
Red circle denotes approximate position of EDX analysis	
Scale	Evidence for silica scale
Alicona surface profiling area 1	Alicona surface profiling area 2

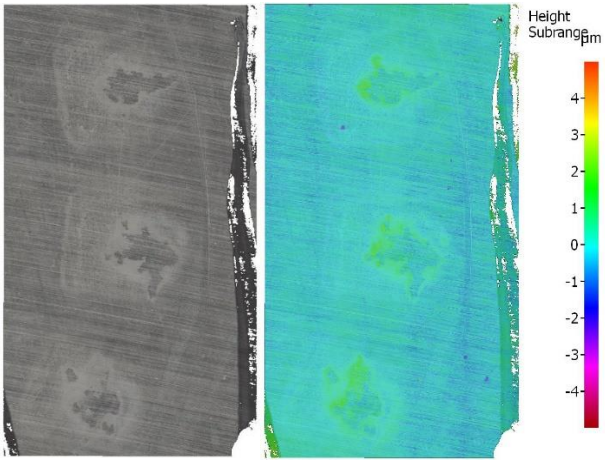	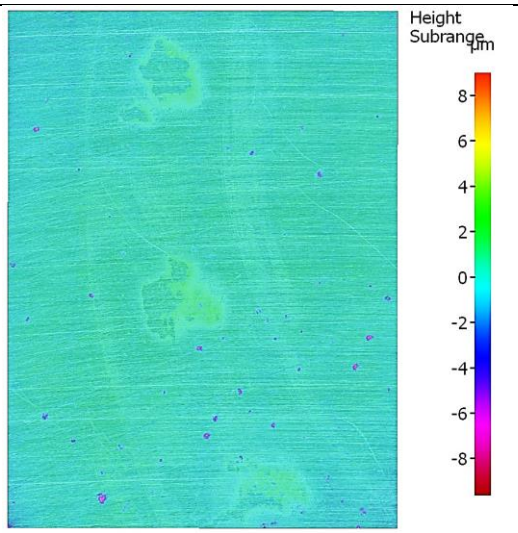
Specimen identity :	2-304-C2
Test temperature:	50^{o}C
Photographs before	Photographs after
	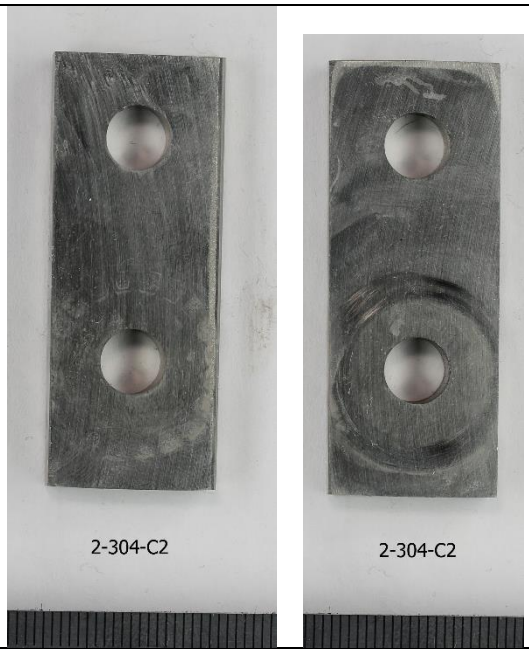
Alicona surface profiling	

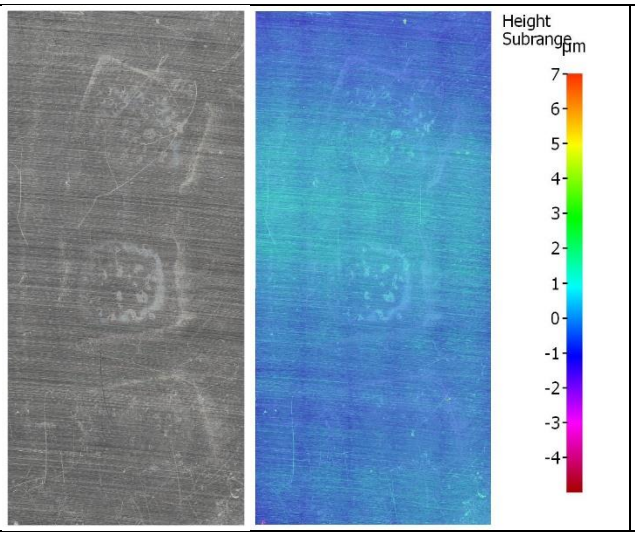
Height
Subrange
µm
7
6
5
4
3
2
1
0
-1
-2
-3
-4

Specimen identity :	1-316-C1
Test temperature:	104^{o}C
Photographs before	Photographs after
SEM images after	EDX analysis after
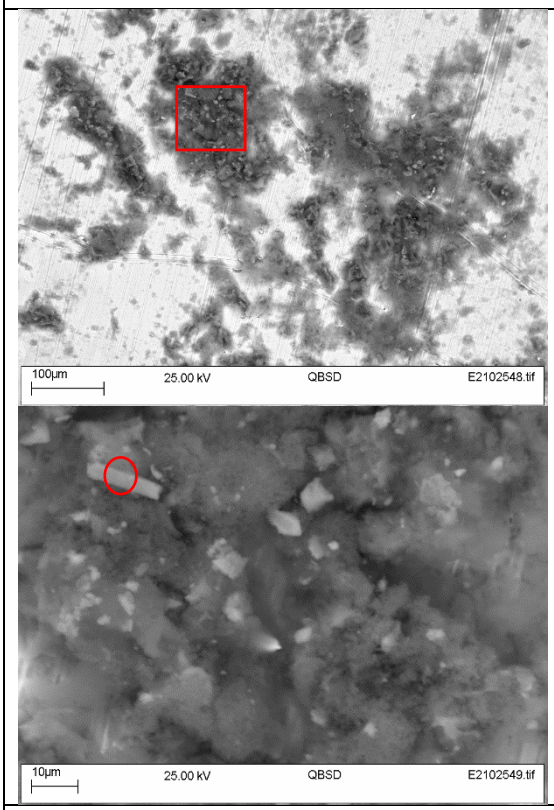	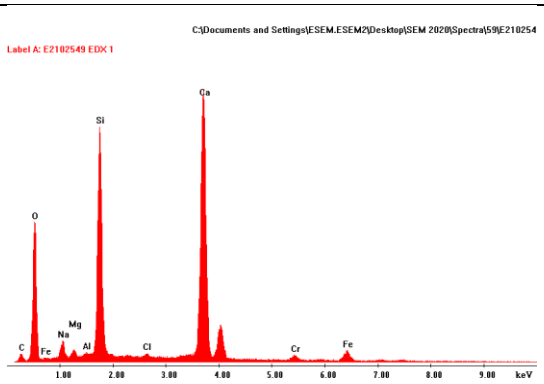
Red square shows location of lower image. Red circle denotes approximate position of EDX analysis	
Scale	Evidence for silica scale and calcium-rich scale

Specimen identity :	1-316-C2
Test temperature:	104^{o}C
Photographs before	Photographs after
	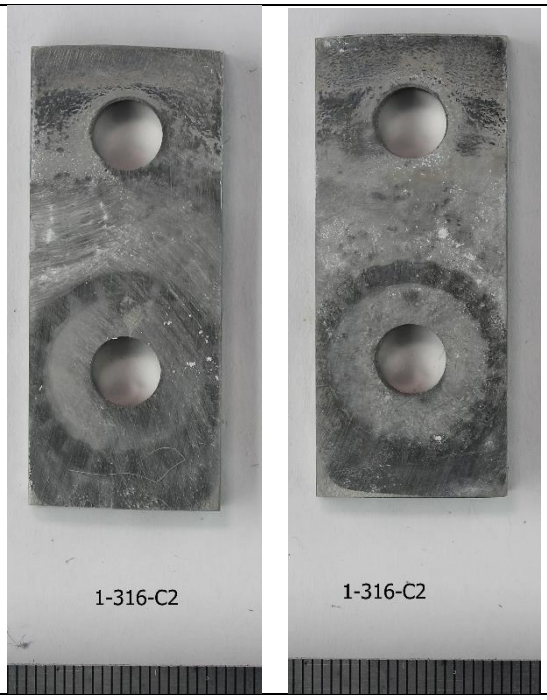

Specimen identity :	2-316-C1
Test temperature:	50^{o}C
Photographs before	Photographs after

Specimen identity :	2-316-C2
Test temperature:	104^{o}C
Photographs before	Photographs after
SEM images after	EDX analysis after
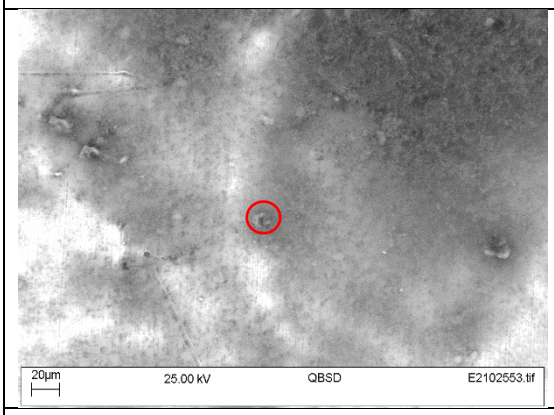	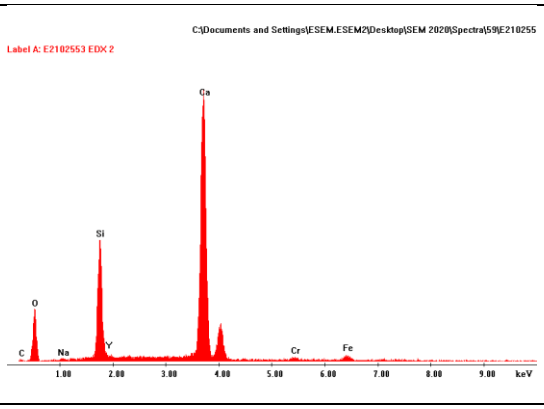
Red circle denotes approximate position of EDX analysis	
Scale	Evidence for silica scale and calcium-rich scale

Specimen identity :	1-Ti-C1
Test temperature:	104^{o}C
Photographs before	Photographs after

Specimen identity :	1-Ti-C2
Test temperature:	104°C
Photographs before	Photographs after
SEM images after	EDX analysis after
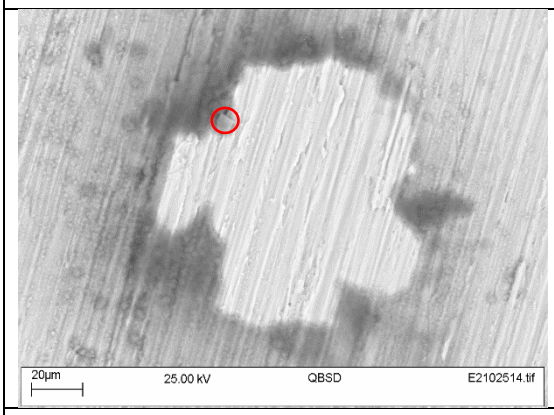	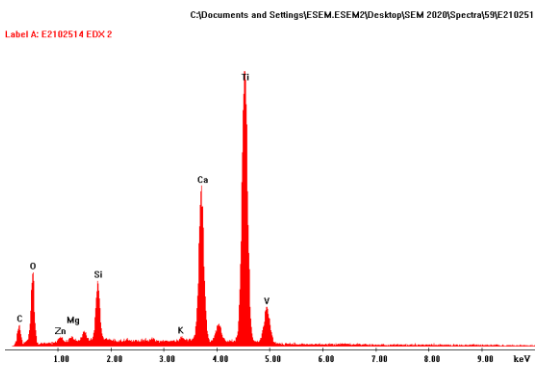
Red circle denotes approximate position of EDX analysis	
Scale	Evidence for silica scale and calcium-rich scale

Specimen identity :	2-Ti-C1
Test temperature:	50^{o}C
Photographs before	Photographs after

Specimen identity :	2-Ti-C2
Test temperature:	50^{o}C
Photographs before	Photographs after
SEM images after	EDX analysis after
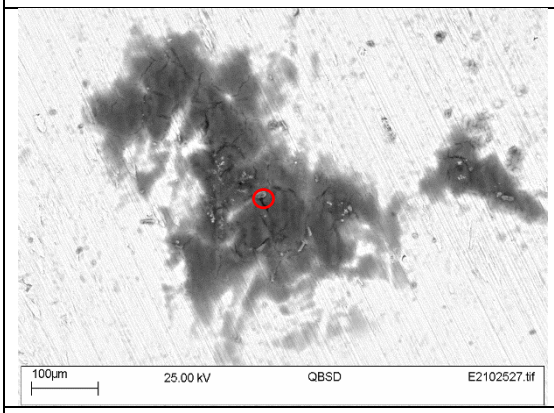	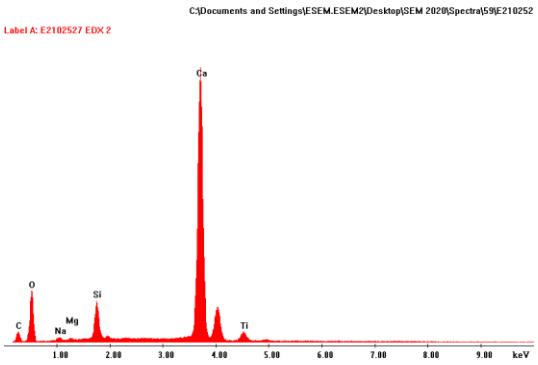
Red circle denotes approximate position of EDX analysis	
Scale	Evidence for silica scale and calcium-rich scale

Specimen identity :	1-UNS-C1
Test temperature:	104^{o}C
Photographs before	Photographs after
SEM images after	
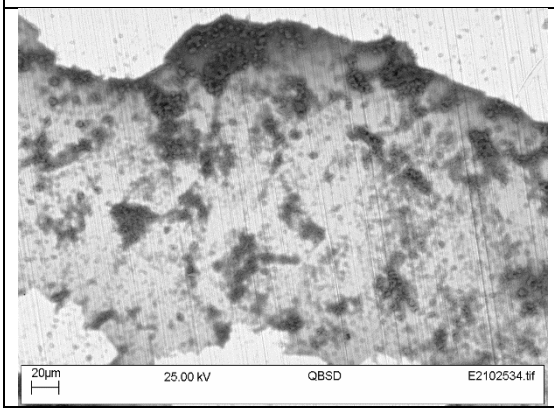	

Specimen identity :	1-UNS-C2
Test temperature:	104^{o}C
Photographs before	Photographs after

Specimen identity :	2-UNS-C1
Test temperature:	50^{o}C
Photographs before	Photographs after

Specimen identity :	2-UNS-C2
Test temperature:	50^{o}C
Photographs before	Photographs after
SEM images after	EDX analysis after
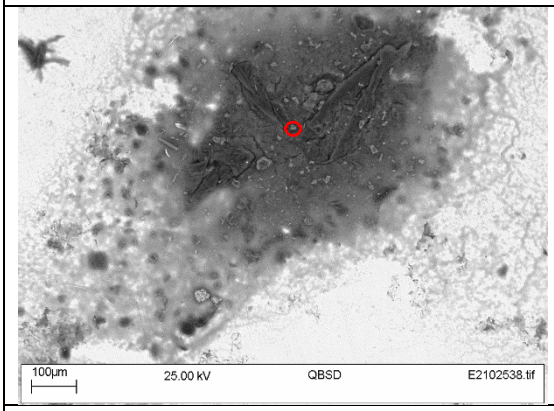	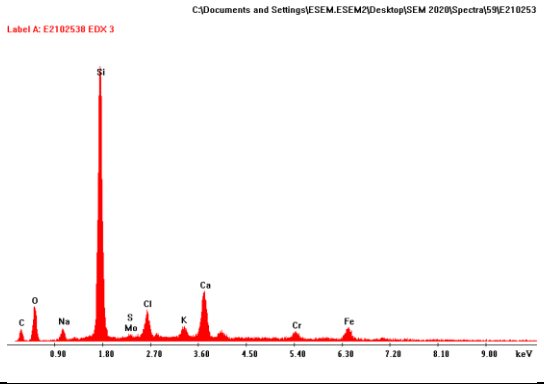
Red circle denotes approximate position of EDX analysis	
Scale	Evidence for silica scale and calcium-rich scale

Appendix B

Results sheets for U-bend specimens

Specimen identity :	1-316-U1
Test temperature:	104^{o}C
Photographs before	Photographs after
	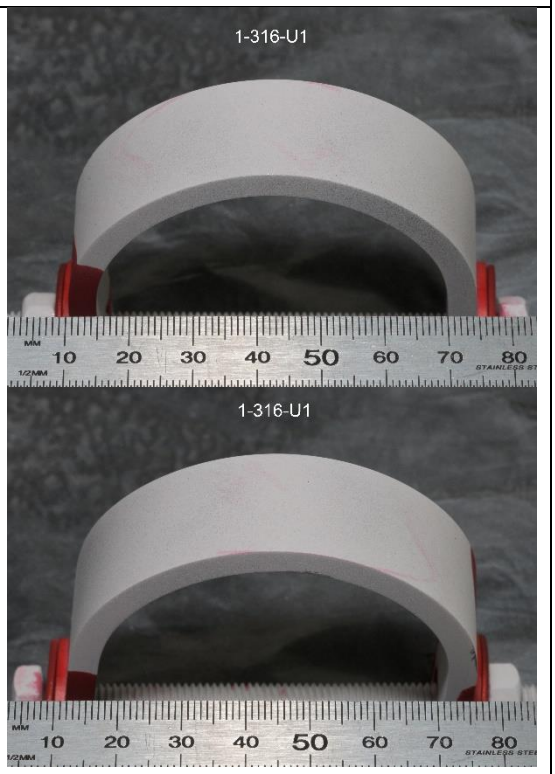
Cracks?	None

Specimen identity :	1-316-U2
Test temperature:	104^{o}C
Photographs before	Photographs after
	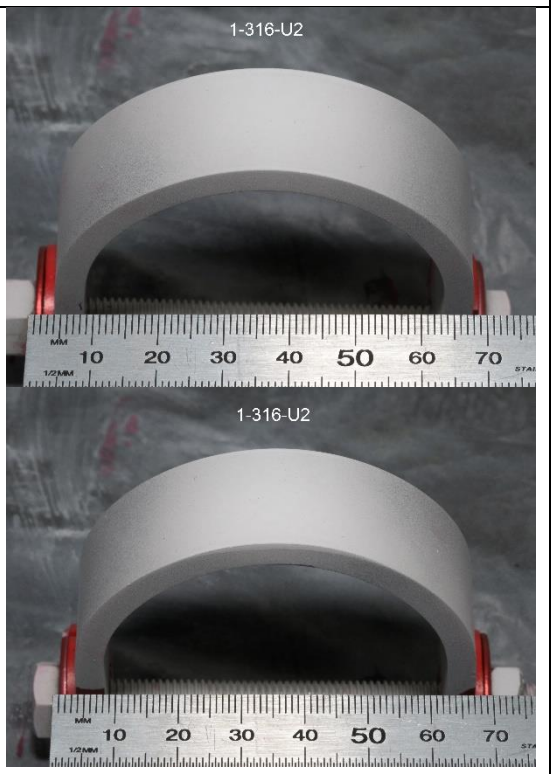
Cracks?	No

Specimen identity :	2-316-U1
Test temperature:	50^{o}C
Photographs before	Photographs after
	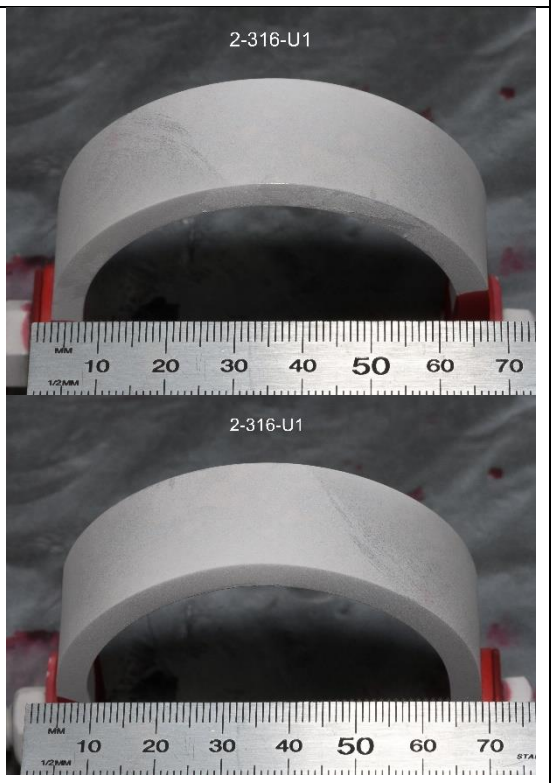
Cracks?	No

Specimen identity :	2-316-U2
Test temperature:	50^{o}C
Photographs before	Photographs after
	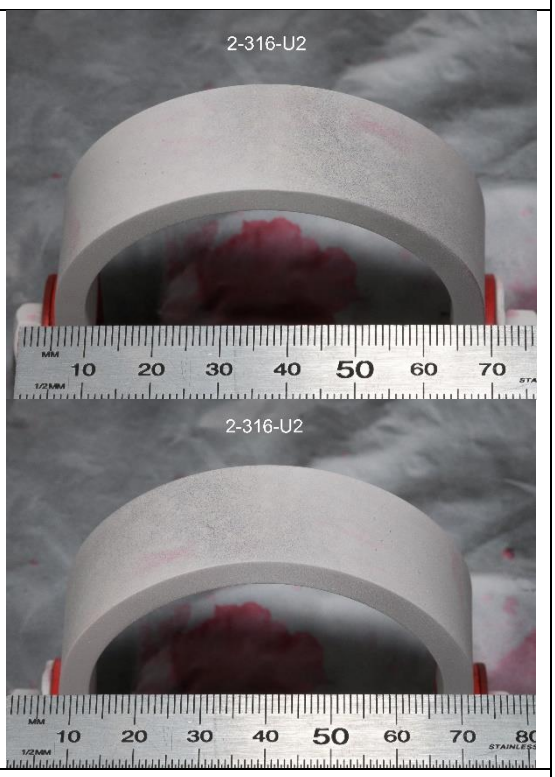
Cracks?	No

Appendix C

Results sheets for potentiodynamic scan specimens

Specimen identity :	PD1-304-P1
Test conditions:	50^{o}C (uninhibited)
Photograph after	

SEM images after	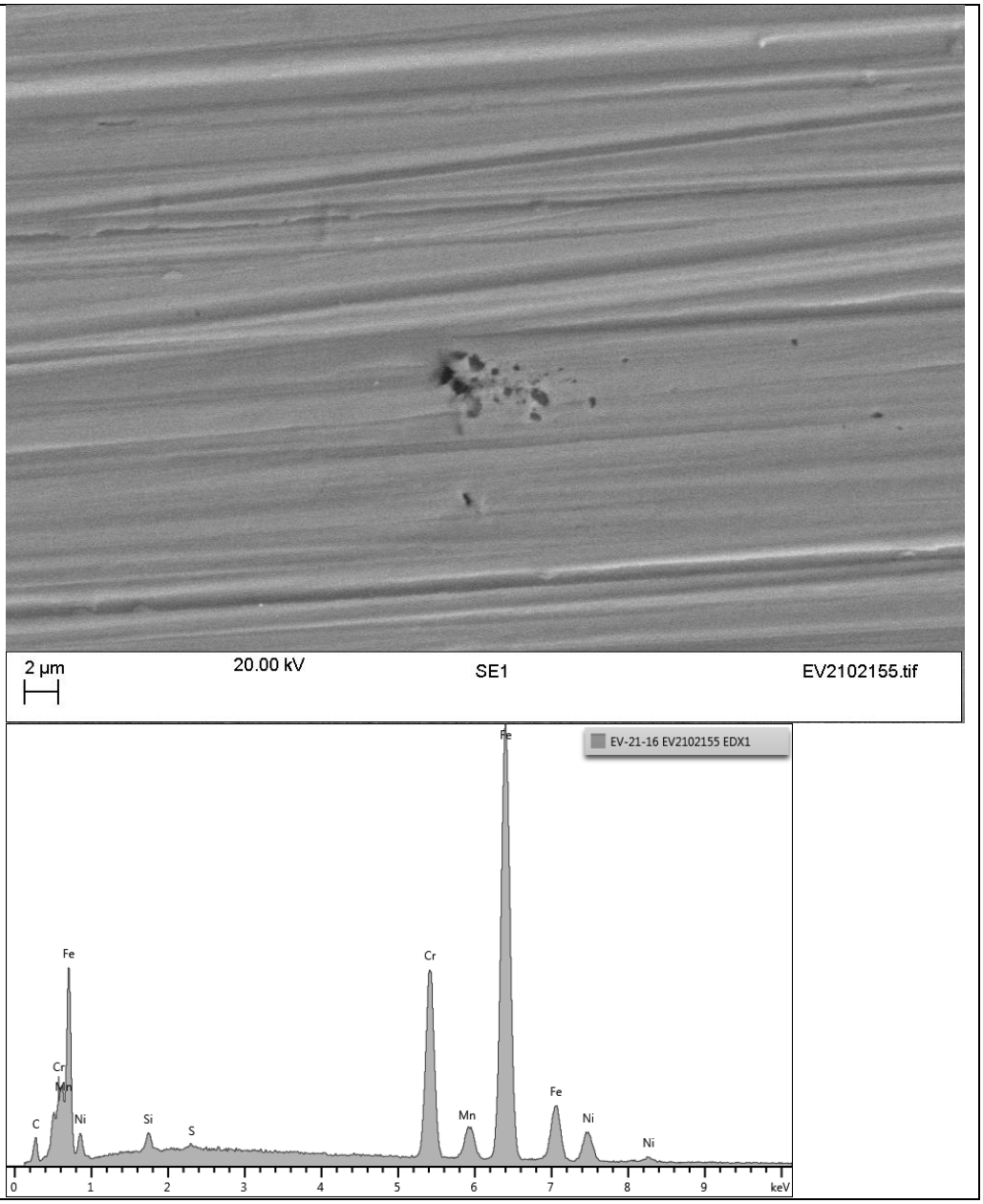

	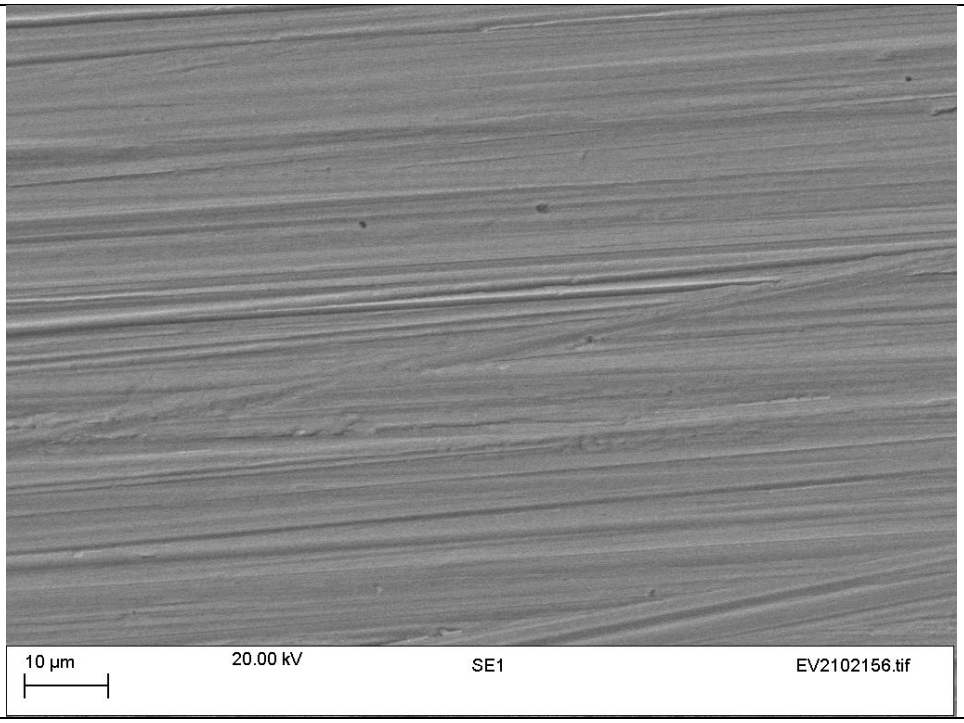
Scale	None observed

Specimen identity :	PD1-304-P2 (SS3)
Test conditions:	50^{o}C (uninhibited)
Photograph after	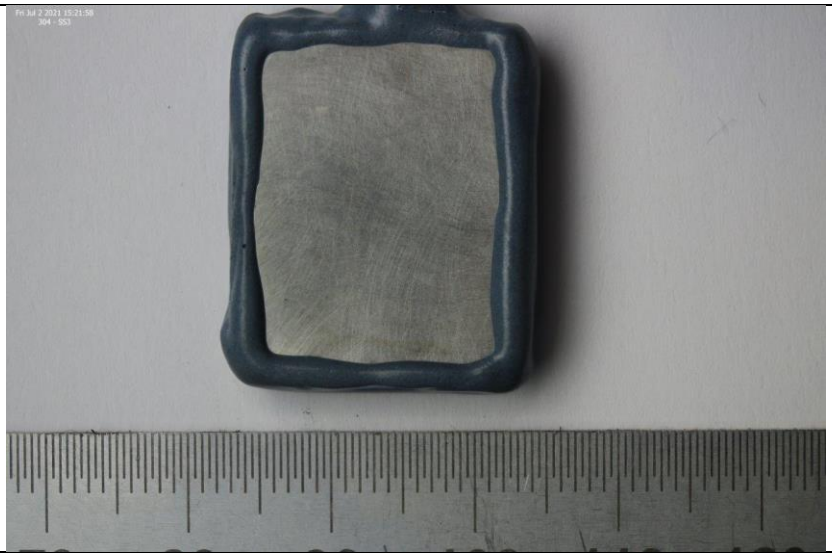

SEM images after	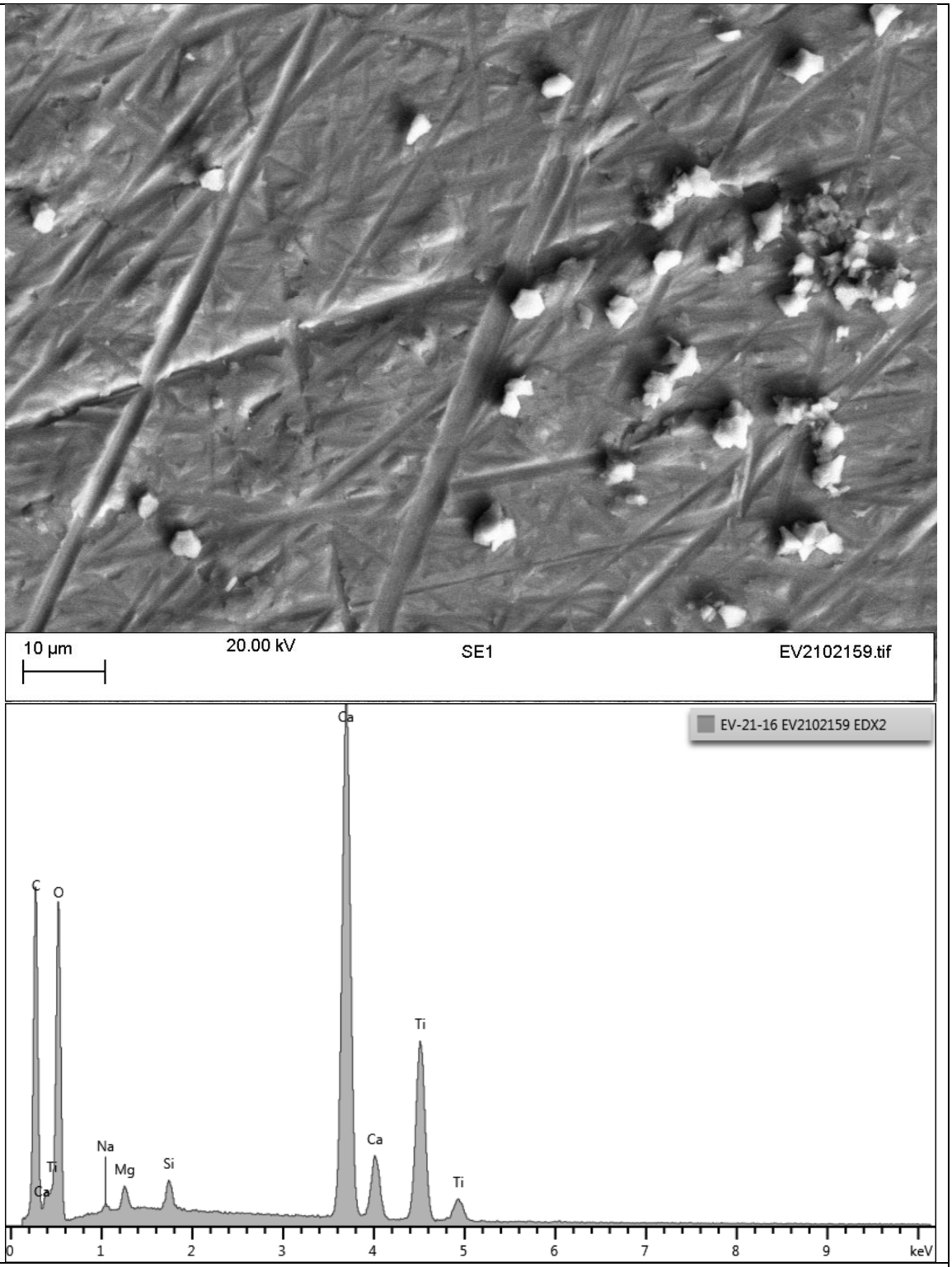
Scale	Very little observed

Specimen identity :	PD1-Ti-P1 (Ti1)
Test conditions:	50°C (uninhibited)
Photograph after	
SEM images after	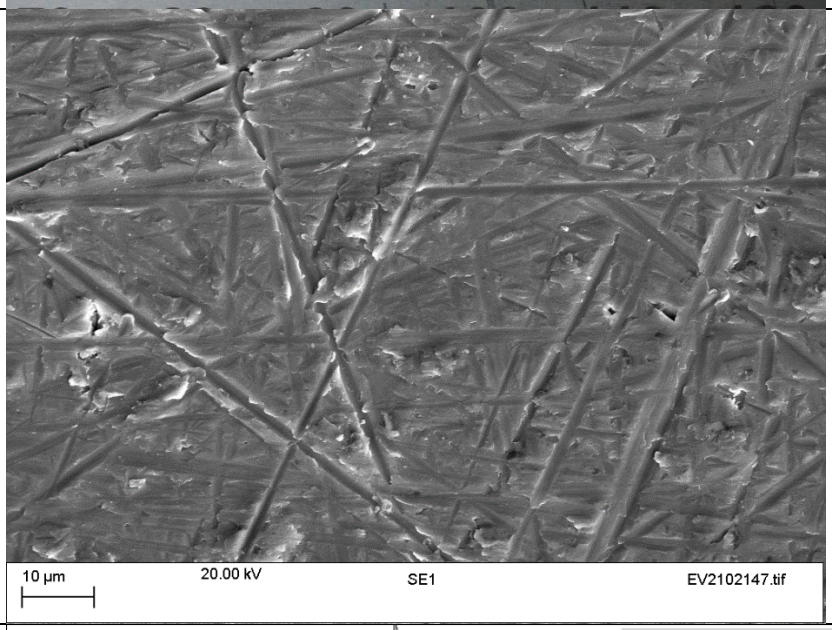
	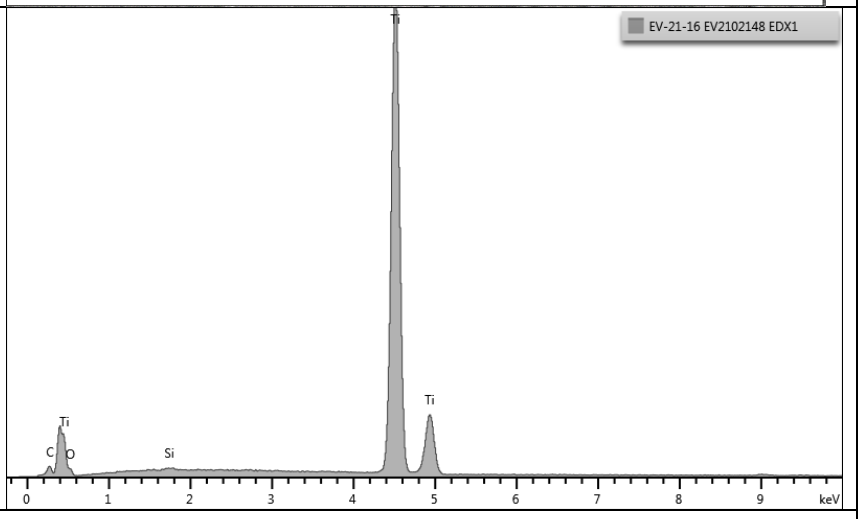
Scale	None observed. Si detected.

Specimen identity :	PD1-Ti-P2 (Ti2)
Test conditions:	50^{o}C (uninhibited)
Photograph after	

SEM images after	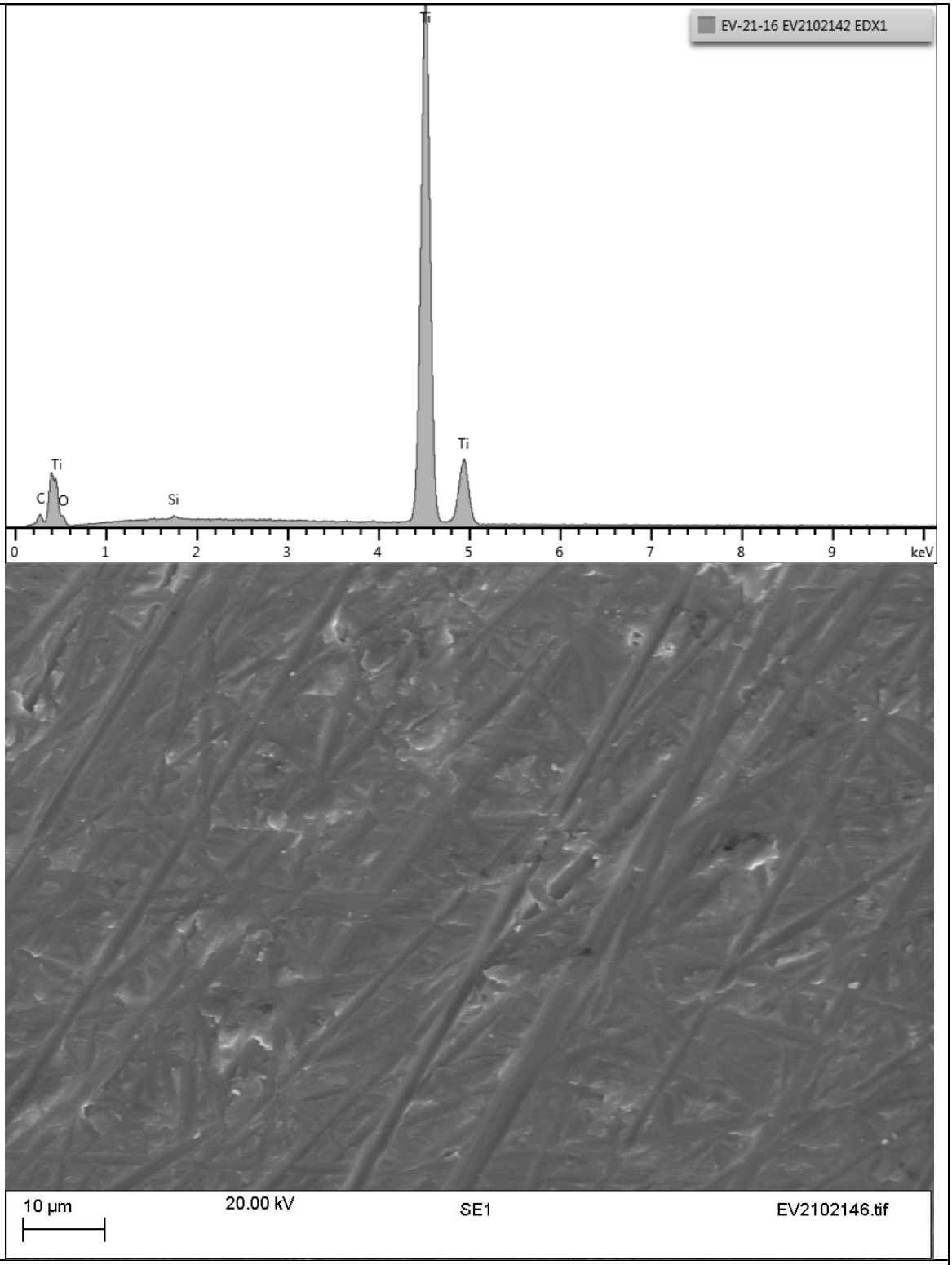
Scale	None observed. Si detected by EDX.